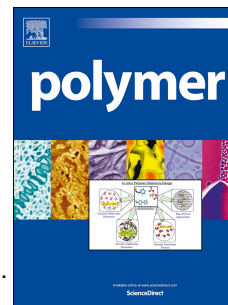# Accepted Manuscript

Interfacial molecular dynamics of styrenic block copolymer-based nanocomposites with controlled spatial distribution

E. Helal, L.G. Amurin, D.J. Carastan, R.R. de Sousa, Jr., E. David, M. Fréchette, N.R. Demarquette

Please cite this article as: Helal E, Amurin LG, Carastan DJ, de Sousa Jr. RR, David E, Fréchette M, Demarquette NR, Interfacial molecular dynamics of styrenic block copolymer-based nanocomposites with controlled spatial distribution, *Polymer* (2017), doi: 10.1016/j.polymer.2017.02.025.

Increasing restriction
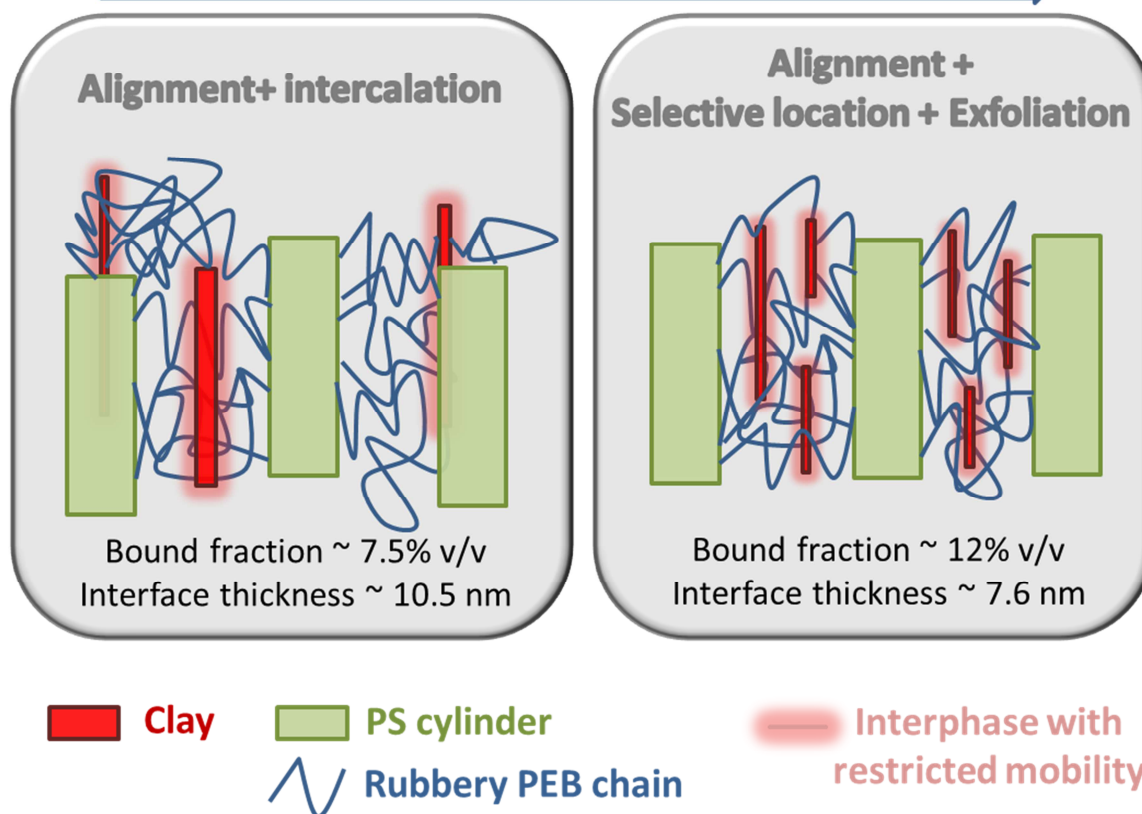
Alignment+ intercalation

Bound fraction ~ 7.5% v/v
Interface thickness ~ 10.5 nm

**Alignment +
Selective location + Exfoliation**

Bound fraction ~ 12% v/v
Interface thickness ~ 7.6 nm

Clay　　**PS cylinder**

Rubbery PEB chain

**Interphase with
restricted mobility**

Interfacial molecular dynamics of styrenic block copolymer-based nanocomposites with controlled spatial distribution

E. Helal [1], L.G. Amurin[1,a], D. J. Carastan [2], R.R. de Sousa Jr. [2], E. David [1], M. Fréchette [3] and N.R. Demarquette [1],*

[1] Mechanical Engineering Department, École de Technologie Supérieure, Montréal, QC, Canada

[a] Current affiliation: MackGraphe Research Center, Mackenzie Presbyterian University, São Paulo, SP, Brazil

[2] Center for Engineering, Modeling and Applied Social Sciences, Federal University of ABC, Santo André, SP, Brazil

[3] Institut de Recherche d'Hydro-Québec, Varennes, QC, Canada

* Corresponding author

Abstract

The dielectric properties of nanocomposites of polystyrene-*b*-poly(ethylene-*co*-butylene)-*b*-polystyrene (SEBS) triblock copolymers containing organically modified clay nanoparticles featuring controlled spatial orientation at the nanoscale: isotropic, totally oriented and partially oriented, have been investigated and correlated with the nanocomposite morphologies. A slow dielectric relaxation process attributed to elastomer chains with reduced mobility confined at nanoparticle/polymer interphase was observed in all the nanocomposites and was found to be dependent on the orientation of nanoclay and polystyrene (PS) domains, the location of clay tactoids as well as the PS block fraction. A dielectric "interfacial" glass transition temperature T_{gi} assigned to this characteristic relaxation was estimated to occur at temperatures ranging between 6 °C and 35 °C depending on the nanocomposite, which is much higher than the bulk rubber phase glass transition temperature, normally lower than -40 °C for the studied block copolymers. Interestingly, the highest T_{gi} were associated with the nanocomposites featuring random or partial orientation and/or selective location of nanoparticles in the rubber phase.

I) Introduction

In nanocomposite materials, controlled orientation of certain anisotropic nanoparticles such as nanoclay[1,2], carbon nanotubes[3] and recently boron nitride nanotubes and nanosheets[4,5] is very beneficial for a wide spectrum of applications requiring excellent mechanical, electrical and/or thermal properties. For example, in the case of mechanical reinforcement, the alignment of nanoclay was reported in several publications to induce an improved mechanical strength in the alignment direction[6]. In the specific case of nanodielectrics, more efficient electron scattering and consequently higher breakdown strength perpendicular to the nanoparticles alignment direction were reported[2,7,8,9]. Simultaneously, nanoparticle alignment was shown to reduce dielectric losses in the direction perpendicular to the main plane of the

aligned nanoparticles[2]. This controlled orientation can be obtained using a wide range of techniques[3] although spatial alignment of nanoparticles according to 2D and 3D patterns is still a challenging field of study[10].

In applications requiring tuned spatial distribution of nanoparticles, the use of block copolymers can be really an asset due to the different nanoscale morphologies these materials present[11,12,13,14,15,16]. To probe the effect of tailored morphology and orientation of such designed nanocomposites on their polymer-filler interactions and implicitly on their final performance, techniques such as broadband dielectric spectroscopy (BDS) are often required[17].

In fact, the performance of polymer nanocomposites in general is governed by the interphase region[18,19] which consists mainly of a bound layer where the motion of macromolecular chains is strongly restricted affecting several properties including dielectric and mechanical properties[19,20,21,22]. The thickness and volume fraction of this interphase usually depend on the geometry of the nanoparticles and their compatibility with the polymer matrix[23,24,25,26]. It was estimated using both experimental techniques[23,25] and molecular dynamics simulations[27,28]. Furthermore, an additional glass transition corresponding to the interfacial polymer chains with restricted mobility was observed in some nanocomposites featuring strong attractive interfacial interactions[20,21,23,24,25,26,27,28,29,30,31,32] and predicted by modeling and simulations[33] as well, for relatively thick bound layers.

The reduced mobility of polymer chains in the interphase region of homopolymer-based nanocomposites has been well investigated during the last years, especially the effect of interaction strength between nanoparticles and the polymer matrix. However, to the best of our knowledge, there is only little literature regarding the interphase region in block copolymer based nanocomposite systems and specifically the effect of the orientation of nanoparticles and block copolymer nanodomains on polymer dynamics in this interphase region. In fact, in the case of nanocomposites prepared from

3

multicomponent polymer matrices, an additional degree of complexity is added to the system as the nanofillers can interact differently with the constitutive components[15,20]. These interactions are usually interdependent and hard to quantify separately. Few studies investigated the dielectric behavior of copolymers and its dependence on chemical and structural factors such as sulfonation[34] and compatibility with different nanofillers. In this context, **Vo et al.**[20] studied the dielectric behavior of styrene-butadiene rubber (SBR) random copolymer filled with three different nanoparticles: nanoclay, silica and carbon black. They reported a new relaxation mode for all three systems attributed to the segmental motion of rubber chains with reduced mobility at the polymer-nanoparticle interface. Moreover, they evaluated an interfacial glass transition temperature T_{gi} associated with this relaxation process. The highest T_{gi} was attributed to the SBR/clay system indicating stronger interaction and better compatibility compared to the two other fillers.

In this work, we investigated polystyrene-*b*-poly(ethylene-*co*-butylene)-*b*-polystyrene (SEBS) thermoplastic elastomer as the block copolymer matrix since it presents excellent features suitable for many applications, such as good mechanical properties[35,36], good resistance to water treeing[37,38] as well as good electromechanical coupling[39]. It is a symmetric triblock copolymer composed of two polystyrene (PS) end-blocks of the same length at the extremities and a poly (ethylene-co-butylene) (PEB) rubber mid-block. Organically modified nanoclays, known for their beneficial effect on mechanical and dielectric properties of polymer nanocomposites including breakdown strength, resistance to surface erosion and reduction of space charge accumulation[2,6,7,8,9,19,40], were added to the thermoplastic elastomer. Four sets of block copolymer nanocomposites containing three different weight fractions of PS phase (0.13, 0.20 and 0.30) were investigated in total. Depending on these ratios and using several fabrication processes, different morphologies were successfully prepared: isotropic vs. totally oriented vs. partially oriented polystyrene nanodomains and clay nanoparticles. Moreover, the

4

degree of exfoliation and location of clay particles inside PS or PEB domains were tailored using a specific SEBS grade with a maleic anhydride (MA) grafted on the PEB block.

In a first step, the orientation of nanoclay and PS nanodomains in the different samples as well as the state of order of the block copolymer were fully characterized by SAXS and TEM. In a second step, the dielectric response was studied as a function of frequency and temperature in order to investigate the influence of the block copolymer tuned architecture on the polymer dynamics, which may affect implicitly the engineering properties such as dielectric losses, breakdown strength and mechanical stiffness, to name a few. The dielectric spectroscopy results were correlated to SAXS and TEM results in order to come up with a template of block copolymer nanodielectrics[41] with controllable morphology and properties suitable for different dielectric applications. In particular, a slower dielectric relaxation mode compared to the main relaxation responsible for the bulk glass transition of the rubbery phase was observed in all nanocomposites and attributed to the segmental motion of rubber chains with reduced mobility located at the polymer-nanoparticle interphase. An interfacial glass transition T_{gi} associated with this new relaxation mode was estimated and used to quantify the interaction strength between the nanoparticles and the polymer chains depending on the configuration, the styrene block content and the location of the nanoparticles in one block or another. Besides, this new dielectric relaxation process, attributed to rubber chains located at the interfacial layer, was also observed in the dynamic mechanical responses of samples prepared from SEBS grade containing 30 wt% of PS block. Finally, the thickness of the interfacial layer was estimated in the range 7-10 nm.

II) Processing

Materials and methods

Four grades of symmetric triblock copolymer SEBS donated by Kraton were used: G1643, G1645, G1652 and FG1901. These grades contain different fractions of PS block ranging from 13 to 30

wt%. Besides, the FG1901 grade contains 1.4-2 wt% of maleic anhydride (MA) group attached to its elastomeric PEB block. All the grades contain 0% of diblocks. More details regarding the physical properties and morphologies of these polymers are reported in Table 1. Montmorillonite clay grade Cloisite 20A purchased from Southern Clay (Gonzales, USA) and modified with dimethyl di(hydrogenated tallow) quaternary ammonium salt, was used as nanofiller for the nanocomposites preparation. More details regarding the physical properties of the polymers as well as the modification and size of clay particles were provided in the previous studies published by co-authors in the same context of research[1,2,42,43]. All the materials studied in this paper were used as received.

Table 1. Properties of SEBS-13, SEBS-20 and SEBS-30

Block copolymer	Grade	PS wt%	MFI (g/10min)	ρ^c (g/cm^3)	T_{OOT}^d (°C)	T_{ODT}^e (°C)
SEBS-20	G1643	20	18[a]	0.9	always cylindrical	> 200
SEBS-13	G1645	13	40[b]	0.9	between 150 and 160 (transition to spherical)	190-200
SEBS-30	G1652	30	5[b]	0.91	always cylindrical	>200
SEBS-30-MA	FG1901[*]	30	22[b]	0.91	always cylindrical	>200
[a] melt flow index measured at 230°C/2.16 Kg, ASTM D1238, provided by the supplier [b] melt flow index measured at 230°C/5 Kg, ASTM D1238, provided by the supplier [c] specific gravity, provided by the supplier [d] order to order transition (OOT) estimated from small amplitude oscillatory shear (SAOS) and small angle X-ray scattering (SAXS) measurements not presented in this manuscript. [e] order to disorder transition temperatures (ODT) estimated from small amplitude oscillatory shear (SAOS) and small angle X-ray scattering (SAXS) measurements not presented in this manuscript. [*] FG1901 grade contains 1.4-2 wt% of maleic anhydride (MA)						

The nanocomposites were prepared by solvent casting, sheet die extrusion or film blowing extrusion to achieve different morphologies. In the case of solvent casting process, the SEBS powder and the nanoparticles were mixed in toluene by magnetic stirring at 60 °C. The mixture was subsequently poured into a Petri dish and left in open air under the fume hood for several days until complete evaporation of solvent. They were subsequently dried in a vacuum oven and annealed according to

specific temperature profiles selected depending on the styrene content, in order to reach equilibrium morphologies[44]. For SEBS-13 and SEBS-20, the sequence: 10 minutes at 50 °C, 30 minutes at 110 °C, 2 hours at 150 °C and 24 hours at 60 °C was used while for SEBS-30 and SEBS-30-MA, the sequence 20 min at 60 °C, 20 min at 100 °C, 20 min at 150 °C and 10 min at 200 °C was used as published in reference[2]. The samples prepared by sheet die extrusion were obtained according to references[1,43]. In a typical procedure, clay nanoparticles were mixed with SEBS in a twin screw extruder equipped with a sheet die, at a temperature profile ranging from 160 to 190 °C for SEBS-20, equal to 150 °C for SEBS-13 and equal to 200 °C for SEBS-30 and SEBS-30-MA and a screw speed of 100 rpm. The films prepared from SEBS-20 by film blowing extrusion were processed in a first step following the same procedure of sheet die extrusion. Subsequently, the samples were processed in a single screw extruder using the same temperature profile and a screw speed equal to 30 rpm. The latter was connected to an annular die with controllable air pressure inside the tube in order to induce lateral elongation and promote biaxial orientation of the block copolymer. In this study, the resulting films were inflated with air at two blow-up ratios: R1=1 and R3=3 in order to initiate respectively uniaxial and biaxial orientation directions. More details regarding this processing method are available in reference[42] published by co-authors. The sheet die extrusion and the film blowing extrusion processes are illustrated in Figure 1.

(a)   **(b)**   **(c)**
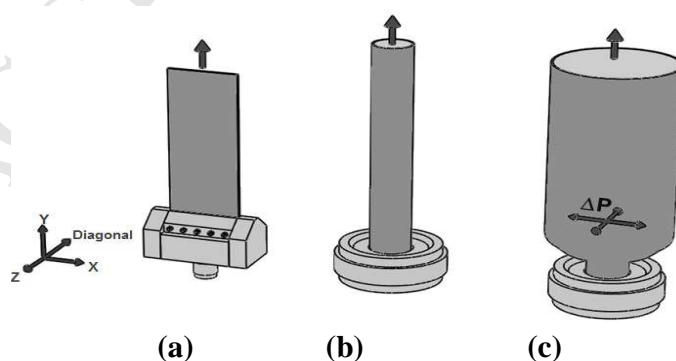
Figure 1. Illustrations showing : (a) sheet die extrusion, (b) film blowing with ratio R1= 1 and **(c)** film blowing with ratio R3= 3 (Coordinate system used as reference is indicated at the left of the figure).

The samples prepared by solvent casting were used without any other treatment for further characterization. The samples prepared by sheet die extrusion and film blowing extrusion were pressed for 2 min at 150 °C for SEBS-13 and SEBS-20 and at 200 °C for SEBS-30 and SEBS-30-MA, under 10 tons before further characterization, in order to have films with comparable thicknesses. The average thickness of all the films was around 550 μm. Short time and relatively low temperatures were used to avoid possible changes in morphology or transition to disordered state (as what will be shown later in the manuscript). The list of samples and their nomenclature are presented in Table 2.

Table 2. Nomenclature of nanocomposites

Polymer	Nanoparticles wt%	Porcessing method	Nomenclature
SEBS-20	0	Sheet die extrusion	SEBS-20-extrusion
SEBS-20	5	Sheet die extrusion	SEBS-20-20A-extrusion
SEBS-20	0	Solvent casting	SEBS-20-solution
SEBS-20	5	Solvent casting	SEBS-20-20A-solution
SEBS-20	0	Film blowing ratio R1	SEBS-20-film blowing R1
SEBS-20	5	Film blowing ratio R1	SEBS-20-20A-film blowing R1
SEBS-20	0	Film blowing ratio R3	SEBS-20-film blowing R3
SEBS-20	5	Film blowing ratio R3	SEBS-20-20A-film blowing R3
SEBS-13	0	Sheet die extrusion	SEBS-13-extrusion
SEBS-13	5	Sheet die extrusion	SEBS-13-20A-extrusion
SEBS-13	0	Solvent casting	SEBS-13-solution
SEBS-13	5	Solvent casting	SEBS-13-20A-solution
SEBS-30	5	Sheet die extrusion	SEBS-30-20A-extrusion
SEBS-30	5	Solvent casting	SEBS-30-20A-solution
SEBS-30-MA	5	Sheet die extrusion	SEBS-30-MA-20A-extrusion

It is worth noting that the morphology and the dielectric response of the materials prepared from the SEBS-30 and SEBS-30-MA grades have been already reported in previous studies[1,2,43]. In particular, it was demonstrated, by TEM and XRD[1], that in the presence of MA, clay particles are mostly exfoliated and located in the PEB phase while in its absence an intercalated clay structure is dominant and clay

tactoids cross PS domains. At increasing clay loading up to 7.5wt%, both the average distance between (100) planes of the cylindrical structures and the diameter of PS cylinders increase[43].

In terms of dielectric properties, it was shown that the alignment of PS cylinders results in an initial decrease of the breakdown strength that was compensated by the improvement induced through the alignment of clay tactoids. The highest increase was equal to 45% compared to unfilled and aligned SEBS-30, at 5wt% loading of clay. In this manuscript, the frequency-domain dielectric response of these samples will be investigated in terms of comparison.

III) Characterization

The morphology of the as-obtained nanocomposites was characterized by small angle X-ray scattering (SAXS) and transmission electron microscopy (TEM). Subsequently, the dielectric properties and the dynamic mechanical properties were characterized by means of respectively broadband dielectric spectroscopy (BDS) and dynamic mechanical analysis (DMA).

Small Angle X-ray Scattering

The SAXS patterns were obtained using Bruker NanoSTAR with 1.5 kV CuKa radiation. The sample-to-detector distance was 650 nm. Besides, bidimensional detectors were used in order to evaluate potential anisotropic features in the samples. The data were analyzed using Fit2D software, without any background subtraction.

Transmission Electron Microscopy

The TEM was performed with a JEOL 2100F microscope. Prior to observations, ultrathin sections of few tens of nanometers were cryo-cut using an ultra-microtome operated at -100 °C and deposited on copper grids. The grids were also stained during 30 minutes with ruthenium tetroxide RuO_4 vapor in order to determine the block copolymer morphology and to evaluate the location of clay nanoparticles.

Broadband dielectric spectroscopy

In terms of dielectric properties, the complex dielectric permittivity of the nanocomposites was measured using a Novocontrol broadband spectrometer. Specimens of 20 mm in diameter were placed between two parallel brass plated electrodes. Measurements swept through a frequency range from 10^{-2} Hz up to 10^5 Hz at a temperature range varying from 25 °C to 90 °C at 5 °C steps, under an rms excitation voltage of 1 V.

Dynamic mechanical analysis

The measurements were performed using a TA Q800 Instrument operated in tensile mode. All the scans were done from -100 °C to 130 °C. The test conditions were as follows: rate of heating equal to 3 °C/min, resonant frequency equal to 1 Hz and strain amplitude equal to 0.1%. The tensile storage modulus (E'), loss modulus (E") and damping factor (tan δ) were evaluated.

IV) Results and discussion

Morphology

SAXS analysis was performed on every sample before and after pressing in order to check the type (cylindrical, spherical, lamellar…) and the stability of the morphology as well as the orientation of both PS domains and clay nanoparticles. The diffraction patterns, before and after pressing, were similar, indicating that the compression molding did not induce any significant change in the initial morphologies. In addition, SAXS patterns were recorded at different temperatures up to 140 °C in order to check for changes in the morphology and state of order that might be encountered during thermal annealing or dielectric spectroscopy scans, as those ones were carried out as a function of temperature. The relative plots indicating peak positions were integrated as well from the 2D patterns. In the following sections, the different samples are analyzed and classified depending on PS block and clay

nanoparticles orientations in three different categories: totally isotropic, totally aligned and partially aligned morphologies.

Totally isotropic morphologies

Isotropic morphologies with totally random orientation of PS nanodomains and clay nanoparticles were obtained in all the samples prepared by solvent casting independently from the polystyrene block content (13, 20 or 30 wt%). Typical diffraction patterns corresponding to SEBS-13-solution and SEBS-20-solution materials are reported in Figure S1 of the ESI file (annex I). The patterns feature concentric rings, in the 3 directions of measurement indicating isotropic orientation of both PS domains and nanoclay. In the case of the pure copolymer, the concentric rings are related to the scattering from PS domains while in the nanocomposite, this scattering is overlapped with more intense scattering from clay nanoparticles. Similar features were observed in nanocomposites prepared from SEBS-30-solution (SAXS data available in the ESI file of reference[2]). TEM micrographs corresponding to SEBS-30-20A-solution nanocomposite are reported in Figure S5 of the ESI file as well (Annex IV). They confirm the isotropic distribution of clay tactoids and PS cylinders in samples prepared by solvent casting method.

Figure 2 presents SAXS radial plots of scattering intensity as a function of scattering vector q corresponding to neat materials and nanocomposites prepared by solvent casting from SEBS-20 and SEBS-13 matrices. Results regarding samples prepared from SEBS-30 were already published in a previous study[2]. The profiles were integrated for 5 different temperatures ranging from 25 °C to 140 °C. In Figure 2(a) and Figure 2(b) corresponding to respectively neat SEBS-20-solution and its nanocomposite, the relative q-positions of Bragg peaks follow the sequence $1:\sqrt{3}:\sqrt{7}$ characteristic of a hexagonally packed cylindrical structure. It can be seen that the intensity of the second peak increased slightly with increasing temperature, as indicated by the arrows, which infers a positive effect of thermal annealing in reaching equilibrium morphologies and consequently improving long-range order[44]. In

Figure 2(c), corresponding to the neat SEBS-13-solution, the same features were observed. However, in the case of the nanocomposite (Figure 2(d)), the first peak was detected at the same position but the second peak was very weak or completely absent. In addition, no obvious improvement was observed with increasing temperature. These results indicate that the state of order is altered in the presence of clay nanoparticles and does not improve with annealing. In particular, this behavior might indicate improved dispersion and degree of intercalation that, in addition to random nanoparticles distribution, help to freeze the block copolymer structure even when subjected to thermal annealing and to reduce the mobility of polymer chains located at the interphase. A higher clay interlayer spacing, d, and consequently intercalation degree has been already reported for nanocomposites prepared by solvent casting from SEBS-13 (d=3.59 nm) compared to nanocomposites prepared from SEBS-30 (d=3.09 nm), both containing Cloisite 15A nanoparticles[45]. This observation will be correlated later with dielectric spectroscopy results.
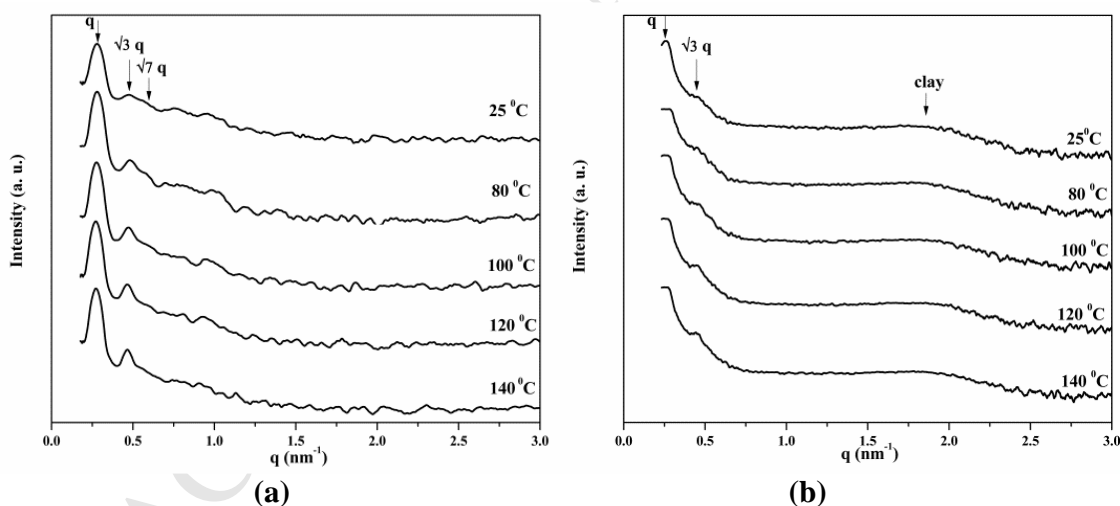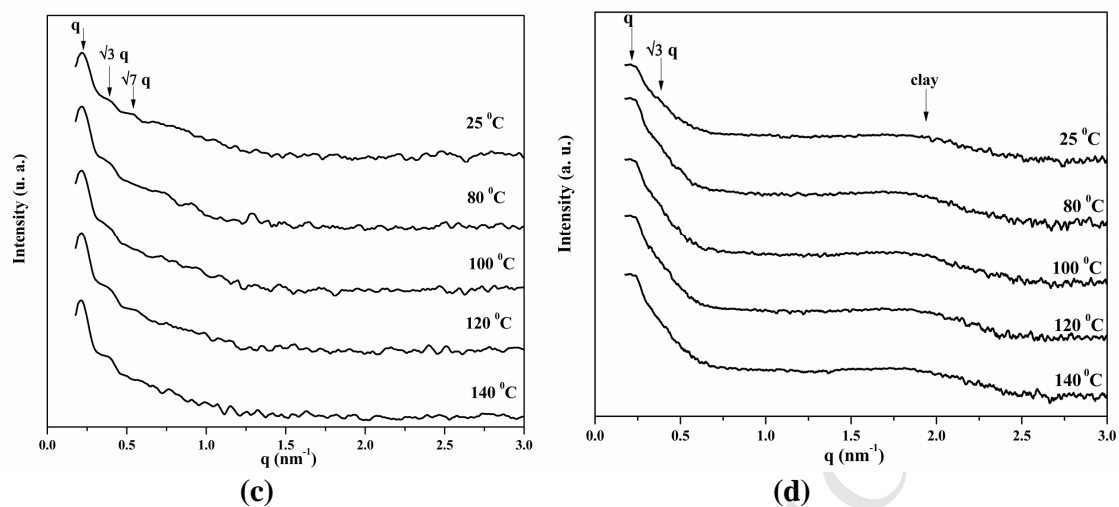
Figure 2. Scattering intensity as function of scattering vector q at different temperatures of: (a) SEBS-20-solution and (b) SEB-20-20A-solution nanocomposite, (c) SEBS-13-solution and (d) SEBS-13-20A-solution nanocomposite

*Totally aligned morphologies*

Diffraction patterns corresponding to samples prepared by sheet die extrusion from SEBS-20, SEBS-30 and SEBS-30-MA are not shown in this manuscript since they exhibit totally aligned morphologies in the extrusion direction. Typical patterns were previously reported by co-authors in reference[1] for SEBS-30 materials. TEM micrographs of SEBS-30-MA-20A-extrusion nanocomposites exhibiting aligned and mostly exfoliated clay layers are reported in Figure S6 of the ESI file (annex V). Aligned morphologies were not obtained in the case of SEBS-13-extrusion as this material has limited tendency to align due to the low fraction of PS block[43]. The case of SEBS-13-extrusion will be treated in the following section within partially aligned morphologies.

Partially aligned morphologies

In addition to totally random morphologies and totally aligned morphologies, some intermediate configurations were successfully achieved depending on the content of styrene and the process used. More specifically, materials prepared from SEBS-20 by film blowing extrusion exhibit two distinct morphologies depending on the blowing ratio: R1=1 or R3=3. Figure 3 shows the diffraction patterns

13

((a)-(b)) and the TEM images ((c)-(e)) corresponding to SEBS-20-film blowing R1 and its nanocomposite SEBS-20-20A-film blowing R1. In particular, the sections examined by TEM were cut perpendicular to the flow direction (i.e. parallel to XZ plane indicated in Figure 1). Diffraction patterns corresponding to neat SEBS-20-R1, presented in Figure 3(a), show evidence of hexagonal packing of PS cylinders in the Y direction while in the X and Z directions, two sets of Bragg peaks can be observed indicating the alignment of the majority of PS cylinders parallel to Y axis (the initial direction of extrusion as indicated in Figure 1). Relative to nanocomposites, diffraction patterns corresponding to SEBS-20-20A-R1 (Figure 3(b)) show strong diffuse spots related to the scattering of nanoclay along the X and Y directions, which indicates dominant alignment of nanoclay parallel to the XY plane (the initial direction of the flow). The presence of maxima in the diffuse spots is characteristic of intercalated nanoclay structure, which was confirmed by X-ray diffraction results reported by co-authors for similar samples[1,43]. TEM images confirm preferential alignment of PS domains and nanoclay in the main direction of the flow (when PS domains appear as small well-defined circles as indicated by the full-line white rectangle in Figure 3(e)). Nevertheless, they reveal the appearance of additional directions of orientation for both PS cylinders and nanoclay, in less important fractions though. In some regions, a fraction of PS cylinders rotated across the thickness (as indicated by the white dotted rectangles in Figure 3(e)). However, the angle of orientation is in most of the cases lower than 90°, meaning that they do not succeed in orienting perfectly along the thickness. Besides, less strong scattering is also observed in the Z direction of the nanocomposite diffraction patterns (Figure 3(b)), which indicates orientation of some clay tactoids in the YZ plane (across the thickness of the sample). This observation is consistent with the TEM image of Figure 3(c) showing that some small clay nanoparticles (indicated by the arrows) are aligned perpendicular to the main orientation of bigger tactoids. This effect could be promoted by the presence of a normal force (parallel to Z axis) induced by the tubular die. However, the

orientation of a small fraction of clay particles in directions other than the main flow direction was reported even for samples prepared by sheet die extrusion[1]. Radial plots of scattering intensity as a function of scattering vector q of the neat material and the nanocomposite are presented in Figure S2 of the ESI file (annex II). The $1:\sqrt{3}:\sqrt{7}$ sequence characteristic of hexagonal structure is observed in both the neat and the nanocomposite confirming the dominance of hexagonal cylindrical structure.
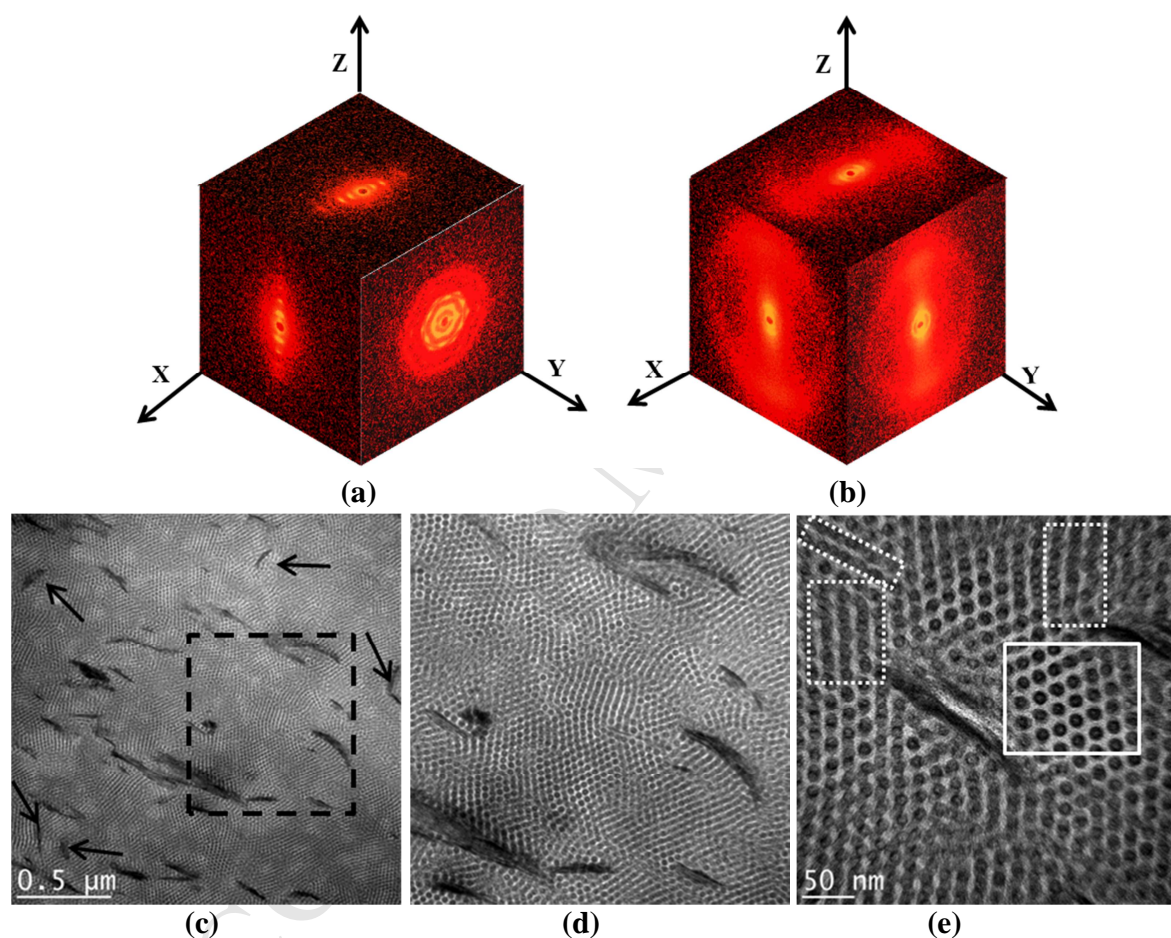
Figure 3. (a)-(b) 2D SAXS patterns of: (a) SEBS-20-film blowing R1 and (b) SEBS-20-20A-film blowing R1, **(c)-(e)** TEM images of SEBS 20-20A- film blowing R1 at 3 different magnifications showing imperfect alignment of PS cylinders and clay tactoids: (d) zoom on the section defined by black square in (c), (e) the white square indicates regions featuring perfect alignment of PS cylinders in the extrusion direction while dotted white rectangles indicate other directions of alignment (PS domains were stained with RuO_4 (dark phase))

Figure 4 shows SAXS diffraction patterns and TEM images of neat SEBS-20-film blowing R3 and its nanocomposite SEBS-20-20A- film blowing R3. The diffraction patterns, presented in Figure 4(a)-(b), reveal the existence of a less perfect hexagonal packing of PS cylinders along the Y axis, compared to SEBS-20- film blowing R1. Besides, Bragg peaks featured in the X and Z directions are wide and almost form concentric rings indicating deviation from the dominant alignment of cylinders along the Y direction (as observed in SEBS-20-R1) and formation of a network of isotropic PS cylinders parallel to the XY plane due to the high blowing ratio and consequently important lateral forces. This observation is further supported by the TEM images presented in Figure 4(c)-(d), showing that more PS domains are oriented in isotropic directions different from the initial flow direction. In Figure 4(b), corresponding to the diffraction pattern of SEBS-20-20A-film blowing R3 nanocomposite, similar features could be observed in the X and Y directions with more intense and narrow scattering indicating more perfect alignment of nanoclay parallel to the XY plane. However, by contrast to SEBS-20-20A-film blowing R1, no specific scattering related to the orientation of clay tactoids in the Z direction is detected. This fact is most likely due to the high lateral forces induced by the R3 blowing ratio that are able to overcome the normal forces applied by the tubular die. Only lateral movements of nanoclay should be possible; thus alignment in the initial direction of the flow is maintained. The radial plots corresponding to SEBS-20-film blowing R3 and its nanocomposite SEBS-20-20A-film blowing R3, presented in Figure S3 of the ESI file (annex II), exhibit again the sequence $1:\sqrt{3}:\sqrt{7}$ characteristic of hexagonal structure. However, it is worth noting that the intensities of the peaks decreased, compared to R1 samples, which might indicate a lack of order due to the increased stretching induced by the high blowing ratio. Moreover, the effect of increasing temperatures in improving the intensities of the peaks is less obvious in these samples, which might indicate a permanent alteration in the block copolymer ordered state due to the important applied deformations. All these observations regarding lack of long

range order and alteration of initial alignment in the extrusion direction are in a good agreement with previous results reported by co-authors in references[43,46], stating that samples where initially aligned PS cylinders are subjected to high strain values in the transversal direction exhibit misalignment due to the rotation of PS domains that tend to align parallel to the deforming force direction. However, this rotation is incomplete due to the competition between the alignment of PS domains and copolymer molecules which don't have enough time to relax. This stretching results as well in breakage of cylinders in shorter domains and reduced long range order. More details regarding these phenomena could be consulted in the cited references[43,46].
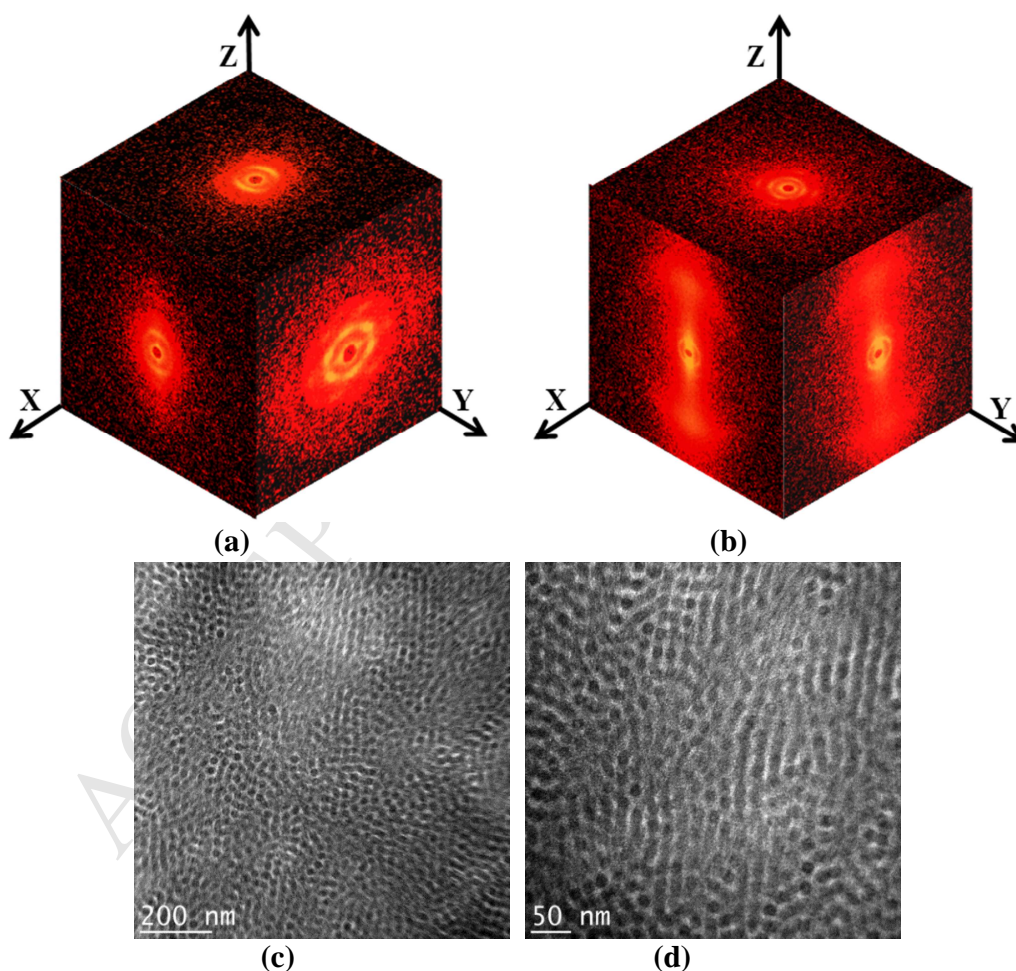
Figure 4. (a)-(b) 2D SAXS patterns of: (a) SEBS-20-film blowing R3 and (b) SEBS-20-20A- film blowing R3 nanocomposite, **(c)-(d)** TEM images of SEBS-20-film blowing R3 at different magnifications (PS domains (darker phase) were stained with RuO_4)

As it was mentioned before, the materials prepared from SEBS-13 matrix by sheet die extrusion do not exhibit totally aligned morphologies[43]. Therefore, their case will be discussed in this section. SAXS diffraction patterns and radial plots corresponding to these samples were integrated, in a similar trend to the previous samples, and reported in annex III of the ESI file (Figure S4).
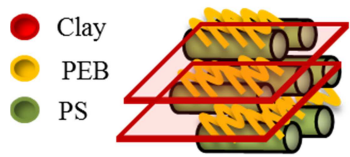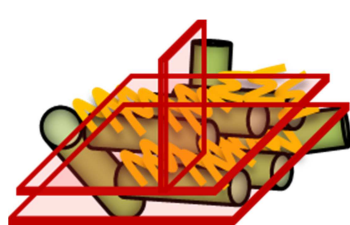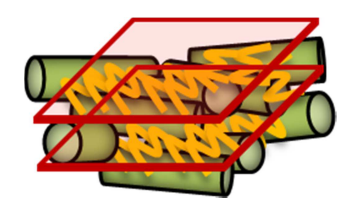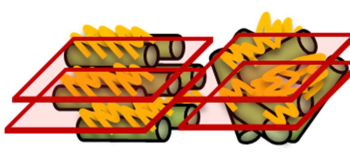
In the diffraction patterns (Figure S4(a)-(b)), only the Z direction is reported for the case of the pure material, as the 3 directions were similar. In particular, concentric rings related to the scattering from the PS phase were observed in the 3 directions, for both the neat copolymer and the nanocomposite. This fact indicates that the majority of PS domains were not able to orient by the applied shear forces during extrusion and remain randomly distributed due to the low polystyrene fraction. However, the scattering from the nanoclay features direction dependence (Figure S4(b)). In fact, 2 strong spots aligned parallel to Z direction corresponding to Bragg peaks associated with scattering from nanoclay were observed in the XZ and YZ planes. These signals indicate the alignment of nanoclays parallel to the extrusion direction. Since this alignment may potentially induce simultaneous orientation of a fraction of PS cylinders, a partially isotropic PS/partially oriented PS configuration will be rather considered for the case of SEBS-13-20A-extrusion nanocomposite. Radial plots (Figure S4(c)-(d)) reveal similar characteristics compared to the samples prepared by solvent casting in terms of dominance of hexagonally packed cylindrical morphology and evolution of order degree with increasing temperature and presence of nanoparticles.

In Table 3, a summary of all the studied samples, a brief description of their morphologies, i.e. the orientation of clay tactoids and PS cylinders, as well as the corresponding illustrations of the morphologies are presented. The nomenclature of the samples is also updated to recall the concluded morphologies. In particular, the samples that are neither totally aligned nor random will be referred to as "partially oriented" to indicate the presence of more than one preferential orientation of PS cylinders or

clay tactoids or both of them. The direction of the applied electric field that was used for dielectric spectroscopy measurements, discussed in the following section, is specified in one of the illustrations as well and remains valid for all the samples.

It is worth noting that since the achieved orientations of PS cylinders and clay particles are dependent on the processing technique, the obtained morphologies are metastable and may change if the samples are subjected to additional processing steps. Therefore, a verification of the morphology is needed if further steps are required. For instance, some studied samples in this manuscript were hot pressed to obtain films of a precise thickness. To avoid potential modification of the morphology, the pressing time and temperature were limited as possible. The stability of the morphology after this step was checked by SAXS.

Table3. Nomenclature, morphology description and morphology sketch of the nanocomposites

	Nomenclature	Morphology description	Morphology sketch
Extrusion	SEBS-20-oriented SEBS-30-oriented SEBS-30-MA-oriented	Uniaxially oriented PS cylinders in the flow direction along Y axis	Clay PEB PS
	SEBS-20-20A-oriented SEBS-30-20A-oriented SEBS-30-MA-20A-oriented	Uniaxially oriented PS cylinders and nanoclay in the flow direction along Y axis	
Solvent casting	SEBS-13-isotropic SEBS-20-isotropic SEBS-30-isotropic	Isotropic PS cylinders	Electric field
	SEBS-13-20A-isotropic SEBS-20-20A-isotropic SEBS-30-20A-isotropic	Isotropic PS cylinders and nanoclay	
Film blowing	SEBS-20-partially oriented R1	Mainly oriented PS cylinders in the flow direction along Y axis Minor fraction oriented across the thickness along Z axis	
	SEBS-20-20A- partially oriented R1	Mainly oriented PS cylinders and nanoclay in the flow direction along Y axis Few PS cylinders and nanoclay oriented across the thickness parallel to YZ plane	
	SEBS-20- partially oriented R3	Isotropic orientation of cylinders in the flow direction parallel to XY plane	
	SEBS-20-20A- partially oriented R3	Oriented nanoclay in the flow direction along Y axis Isotropic orientation of cylinders in the flow direction parallel to XY plane	
Extrusion	SEBS-13- partially oriented	Partially isotropic PS cylinders Partially oriented PS cylinders in the flow direction along Y axis	
	SEBS-13-20A- partially oriented	Partially isotropic PS cylinders Partially oriented PS cylinders in the flow direction along Y axis Oriented nanoclay in the flow direction along Y axis	

20

Dielectric properties

The complex dielectric permittivity of an insulating material measures its response to an applied electrical field either through polarization mechanisms or charge carrier fluctuations[17]. The corresponding equation is described in annex VI of the ESI file (equation (S1)).

In this manuscript, the dielectric response of the studied materials has been characterized as functions of frequency and temperature. To better understand the origin and the dynamics related to the relaxation modes observed in each material as well as to evaluate the contribution from charge fluctuations, depending on the orientation of PS cylinders and nanoclay, dielectric permittivity spectra of all nanocomposites were fitted according to equation (S2)[17] , described in annex VI of the ESI file, which comprises a power law term to describe the contribution of charge fluctuations[47,48] and a sum of Havriliak-Negami (HN) functions to take into account the observed dipolar dielectric relaxation processes[17,20,21,49]. There are as many terms in the sum of HN functions as there are observed relaxations. Commercially available software was used to obtain the curve-resolved spectra. Both real and imaginary parts of the dielectric permittivity were considered for the fitting, computed based on nonlinear procedures. However, only curve resolved spectra of the imaginary part are reported in the manuscript. More details regarding the fitting procedure are available in annex VI of the ESI file.

It is worth noting that the fitting of the experimental data to equation (S2) was applied to the dielectric spectra of all nanocomposites in the temperature range from 40 °C to 90 °C, where no specific molecular relaxation processes are supposed to occur in the neat material as reported by previous studies[34,50]. In fact, the segmental relaxation associated with the bulk glass transition of the rubber phase is too fast and could not be observed within this temperature window while the relaxation associated with the glass transition of PS phase is too slow and could not be observed either.

Figure 5 shows the imaginary part of the dielectric permittivity of neat SEBS-20 (Figure 5(a)) and its nanocomposites (Figure 5(b)-(e)), prepared by the three processing techniques mentioned previously, at different temperatures ranging from 30 °C to 90 °C. Only SEBS-20-partially oriented R3 was presented in Figure 5(a) as the other control samples, without clay, prepared by sheet die extrusion or solvent casting feature similar dielectric behavior. Moreover, for the sake of simplicity, the real part of the dielectric permittivity is not reported in this manuscript since relaxation phenomena are observable in both real and imaginary parts and the analysis of the imaginary part is more straightforward. Typical spectra of real part of the dielectric permittivity could be consulted in Figure S8 of the ESI file (annex VIII).

The real part of the dielectric permittivity of the neat SEBS is almost frequency independent and nearly equal to 2.35. At increasing temperatures, both the real and the imaginary parts of the dielectric permittivity of the neat copolymer remained equal to or slightly decreased below the value exhibited at room temperature (as it could be seen in the insert of Figure 5(a) and Figure S8 of the ESI file). This decrease is probably related to the decreased polymer density at increasing temperatures, which is linearly affecting the relative permittivity[51]. In addition, the high frequency relaxation peak related to the glass transition of the rubber phase shifts towards higher frequencies with the temperature increase (not observed in the studied range) causing a decrease of the dielectric losses in the 10^3 to 10^5 Hz frequency window.

In all the nanocomposites, both ε' and ε'' increased simultaneously compared to neat SEBS (Figure 5 of the manuscript, Figure S7 and Figure S8 of the ESI file), up to orders of magnitude, particularly at low frequencies and high temperatures, indicating an important contribution originating from the inclusion of nanoclay to the low frequency dispersion[47,48]. In particular, a pronounced increase is observed in the isotropic samples featuring random clay tactoids distribution compared to the samples

where clay particles are aligned perpendicular to the electric field (Figure 5(e) compared to Figure 5(b)-(d)). This behavior is most likely attributed to an anisotropic nature of clay conductivity which might be considerably lower across the nanoplatelets thickness than along their surface and the interlayer spacing, covered by a diffuse ionic layer[7,52]. Another possible contribution to this remarkable increase of permittivity could be attributed to the presence of a fraction of polar organic solvent that was trapped during the solvent casting process used for the preparation of the isotropic samples.

It is worth noting that there is only little information regarding the experimental values of dielectric permittivity and electrical conductivity of nanoclay which strongly depends on the type of surface modification and the density of adsorbed cations[53]. The dielectric properties of an organically modified clay tactoid, similar to the one used in this study, were estimated through modeling by **David et al.**[7]. In particular, the pure direct current conductivity of clay was estimated to be equal to 10^{-9} S/m.
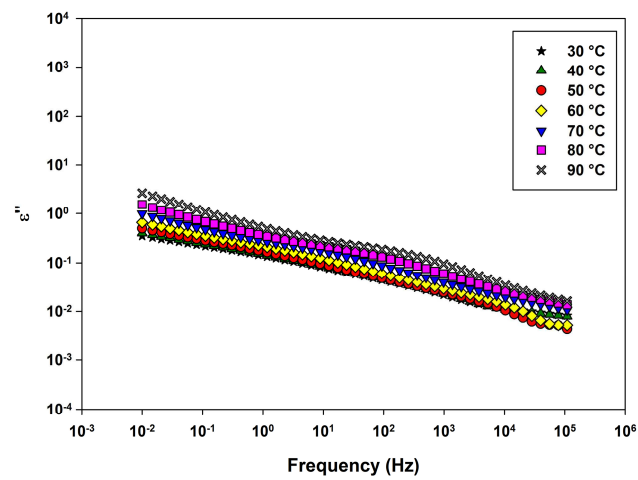
The fitting of the dielectric permittivity to equation (S2) confirmed that all the nanocomposites exhibit, in addition to the charge fluctuation term, two relaxation modes that were not observed in neat materials. Similar behavior was reported in the literature for clay nanocomposites in general[7,8,54] and clay/rubber nanocomposites specifically[20,21]. The charge fluctuation term is few orders of magnitude higher in the isotropic nanocomposite. In particular, considering the case of pure electronic conductivity in the fitting process (n=0 in equation (S2)), the values of conductivity σ_0 are in the range 10^{-9} to 10^{-11} S/m for the isotropic nanocomposite while they are in the range 10^{-12} to 10^{-14} S/m in the case of oriented and partially oriented nanocomposites. In terms of relaxations, the first peak is located at low frequencies and is often overshadowed by the low frequency dispersion. It is attributed to Maxwell-Wagner-Sillars (MWS) polarization and is at the origin of the step-like increase observed in the real part of dielectric permittivity at the lowest frequencies. The second relaxation process was observed at intermediate frequencies and is shifted to higher frequencies at increasing temperatures. It is at the origin

of the second step-like increase observed in real permittivity at intermediate frequencies. This additional relaxation could be probably due to a MWS process from water absorbed at nanoparticles surface for instance[17,54] or to local segmental relaxation of rubber chains with reduced mobility located at polymer/clay interfaces, which is slower than the main segmental relaxation responsible for the bulk T_g of the elastomer[20-32]. In the case of SEBS, the dynamic T_g of the PEB rubbery block is in the vicinity of -40 °C, depending on the polystyrene block fraction[43,55]. An example of this fit is presented in Figure 5(f). It corresponds to the dielectric loss spectrum of SEBS-20-20A-partially oriented R3 nanocomposite at 75°C (Different colors are used to denote the different contributions).

Moisture absorption in nanocomposites was reported several times in literature, especially for epoxy-based nanocomposites containing polar groups and/or nanoparticles modified with functional groups of relatively low hydrophobicity[54,56,57]. The absorbed water could form an interfacial conductive layer between the nanoparticles and the matrix material, which gives rise to an interfacial loss process[17]. In this study, the hypothesis of moisture absorption is discarded as SEBS is an apolar copolymer exhibiting very low water uptake and Cloisite 20A, the organically-modified clay used, features high hydrophobic character due to its dimethyl ditallow ammonium based modifier[58]. It has also been reported that 24 hours of immersion in water was not found to have a significant impact on the dielectric response of HDPE containing 10wt% of organically-modified clay[59].
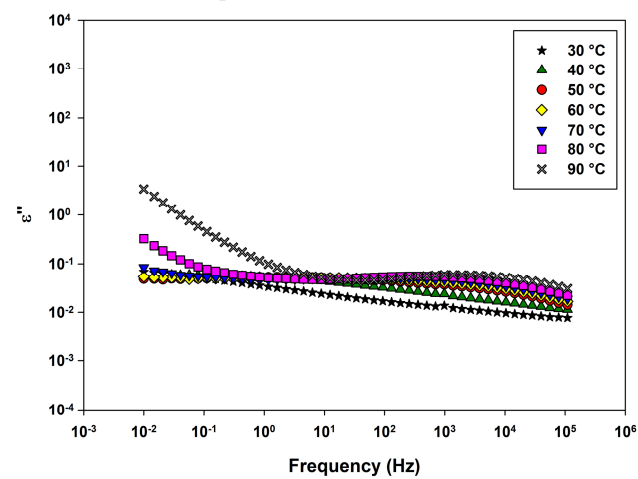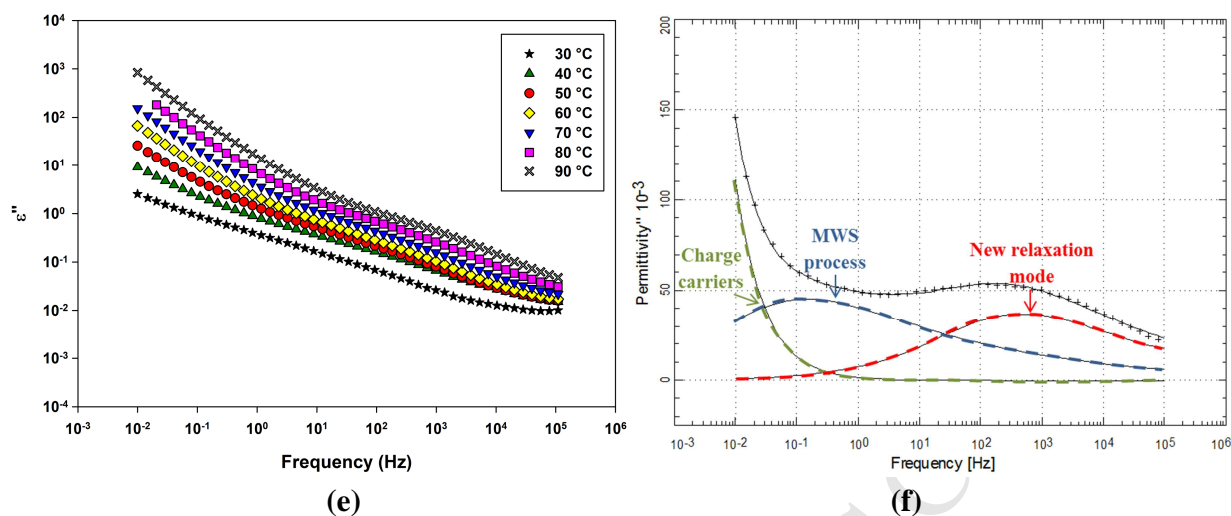
(a)

(b)

(c)

(d)

(e)

(f)
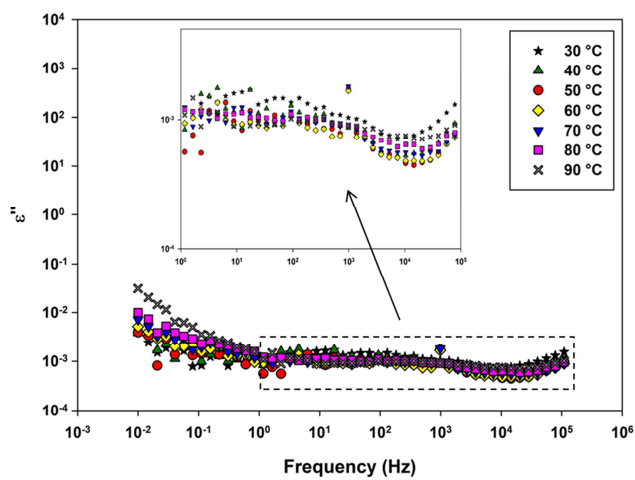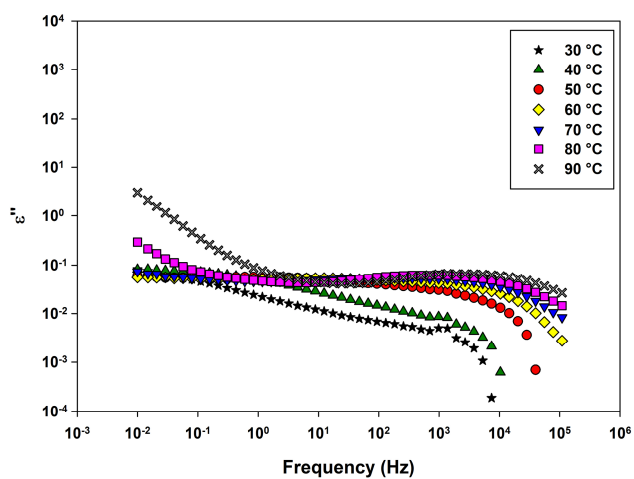
Figure 5. Imaginary part of the dielectric permittivity as a function of temperature of: (a) neat SEBS-20-partially oriented R3, (b) SEBS-20-20A-oriented, (c) SEBS-20-20A- partially oriented R1, (d) SEBS-20-20A-partially oriented R3, (e) SEBS-20-20A-isotropic and (f) an example of the fitting corresponding to SEBS-20-20A-partially oriented R3 at 75 °C (Different colors are used to denote the different contributions)

Effect of orientation on dielectric behavior

In order to confirm the origin of the second relaxation process, i.e. glass transition of the interfacial rubbery chains with reduced mobility, and to evaluate the effect of PS cylinders and nanoclay orientations on it, the temperature dependence of the relaxation times relative to this process was analyzed. At each temperature, the relaxation time corresponding to the peak maximum frequency was determined from the HN fit according to equation (S3)[17], described in annex VI of the ESI file.

Figure 6 presents the relaxation times relative to the relaxation process observed at intermediate frequencies as a function of inverse temperature for all the nanocomposites prepared from SEBS-20. The temperature dependence of the relaxation times is well described by the empirical Vogel-Fulcher-Tammann (VFT) equation (equation (S4) described in annex VI of the ESI file), which is usually used to

26

fit the segmental relaxation process related to the bulk glass transition[17]. This behavior supports the hypothesis of molecular relaxation at the origin of the second peak observed at intermediate frequencies. The parameters of the VFT fit of each nanocomposite were computed and listed in Table 4.

Besides, a dielectric "interfacial" glass transition temperature T_{gi} was associated to this relaxation mode in analogy with the glass transition temperature assigned to the segmental relaxation of the bulk rubber phase. This temperature was estimated by extrapolating the VFT fit to an extremely long relaxation time, conventionally chosen equal to 100 seconds[17,20]. The calculated temperatures are listed in Table 4 as well.

In particular, the obtained values of the VFT parameters τ_0, B and T_0 related to this new relaxation mechanism governing the mobility of the interfacial chains are in the same range of those reported previously by several groups for different rubber based nanocomposites where a similar phenomenon was observed such as **Vo et al.**[20] for their SBR based nanocomposites, **Lin et al.**[23] for their Poly(vinylacetate)/silica nanocomposites and **Wu et al.**[60] for their Butadiene-Styrene-Vinyl pyridine rubber/Graphene Oxide nanocomposites.

In addition, the kinetic fragility index F, which characterizes how rapidly the dynamics of a material slow down as it is cooled toward the glass transition temperature, was estimated according to equation (S5)[61,62], described in annex VI of the ESI file. Considering that the behavior of the relaxation time as function of temperature is described by the VFT equation, the derivative could be calculated for each sample. The calculated values of F are reported in Table 4 as well.

It could be seen from Figure 6 that the sample with isotropic orientation features the highest relaxation times and consequently the slowest dynamics while the oriented nanocomposite exhibits faster dynamics. Interestingly, both partially oriented nanocomposites R1 and R3 exhibit even more reduced

relaxation times especially toward the highest studied temperatures. This speed up of chain dynamics was reported in literature for rubber-based nanocomposites at increasing clay and graphene oxide nanoparticles loadings and it was attributed to suppression of cooperativity of polymer chains confined in the intercalated structures, when the confinement volume becomes comparable to that of the cooperative rearranging regions[21,60,63]. Moreover, at decreasing temperatures, the partially oriented samples feature increased dependence on temperature and converge to the behavior of the isotropic nanocomposite. This special behavior might be an indication of strong intermolecular coupling, i.e. the relaxation times diminish more rapidly with increasing temperatures[64,65,66].

The analysis of the calculated interfacial glass transition temperature T_{gi} reveals that the new relaxation process is located, depending on the nanocomposite configuration, in the temperature range between 26 and 35 °C; much higher than the bulk glass transition of PEB phase which will be studied by DMA analysis in a following section. Furthermore, this T_{gi} seems to depend as well on the orientation of both nanoclay and PS cylinders, as it was expected from the observed difference of the dependence of relaxation times on temperature. Overall, the oriented samples prepared by extrusion exhibit the lowest interfacial glass transition temperature, which might indicate that this controlled configuration helps decreasing the induced molecular chains confinement, and consequently the interaction strength in the interphase region. In fact, the isotropic and the partially oriented samples exhibit characteristic T_{gi} up to 9 degrees higher, which is in good agreement with their morphology featuring more complex patterns and disorder. Indeed, the calculated values of fragility index confirm that partially oriented and isotropic samples feature more fragile behavior and consequently higher intermolecular coupling and interaction strength at the interface.
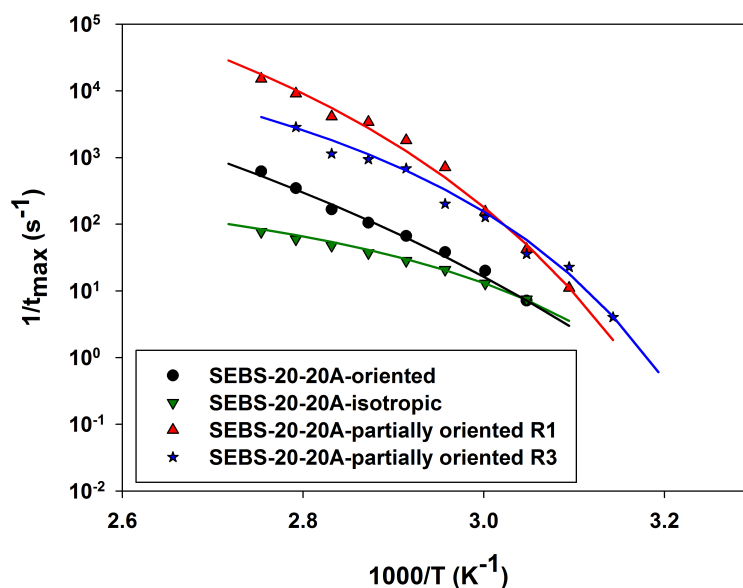
Figure 6. Temperature dependence of the relaxation times corresponding to SEBS-20 nanocomposites prepared by different processes: symbols correspond to relaxations times retrieved from the HN function and solid lines correspond to VFT fitting.

Table 4. VFT fitting parameters corresponding to SEBS-20 based nanocomposites

Samples	τ_0 (s)	T_0 (K)	B (K)	T_{gi} (K)	F
SEBS-20-20A-partially oriented R1	4.24E-09	271	869	308	87.8
SEBS-20-20A-partially oriented R3	7.33E-07	280	483	306	95.8
SEBS-20-20A-oriented	1.05E-08	229	1620	299	43.7
SEBS-20-20A-isotropic	6.00E-04	285	232	305	80.1

While T_{gi} is indicative of interaction strength, the dielectric strength of the related relaxation mechanism partially corresponds to the number of interacting dipoles involved in the relaxation process, according to the Debye-Fröhlich-Kirkwood theory[17,67,68]. Therefore, a weaker signal is expected to correspond to less interacting polymer compared to a stronger signal. However, it is difficult to compare quantitatively the signal strength among different samples due to some inaccuracies such as in sample thickness measurements. Thus, this parameter could be considered only qualitatively[20]. Illustrative values of dielectric strength corresponding to each sample are reported in Table 5, at two temperatures: 60 °C and 80 °C. It could be seen that the isotropic sample featured the highest dielectric strength values followed by the partially oriented samples in a second level while the oriented sample featured the

lowest values. Hence, the amount of polymer chains with restricted mobility, located at the interphase, is larger in these samples featuring complex morphologies, which is consistent with the conclusions made earlier from T_{gi} results.

Table 5. Dielectric strength of SEBS-20 based nanocomposites at 60 °C and 80 °C

Samples	Δε at 60 °C	Δε at 80 °C
SEBS-20-20A-partially oriented R1	0.369	0.379
SEBS-20-20A-partially oriented R3	0.383	0.345
SEBS-20-20A-oriented	0.295	0.273
SEBS-20-20A-isotropic	0.540	0.528

Effect of styrene content and diameter of PS cylinders

In order to elucidate the effect of nanoclay interaction with each phase of the block copolymer on the polymer chain dynamics at the interphase region, comparisons were made between isotropic samples and oriented samples prepared from the different block copolymer matrices containing respectively 0.13, 0.2 and 0.3 polystyrene fractions. The dielectric spectra of the samples prepared from SEBS-30 are available in reference[2] while the results related to SEBS-13 based nanocomposites are reported in Figure S7 of the ESI file (annex VII). Examples of the fitting according to equation (S2) of the ESI file, for each type of nanocomposite are presented in Figure 7 (Different colors are used to denote the different contributions). In particular, nanocomposites prepared from SEBS-13 are well fitted by a power law term and two HN functions (similar to previous samples prepared from SEBS-20), such as the example reported in Figure 7(a), corresponding to SEBS-13-20A-isotropic. SEBS-30-20A nanocomposites, in comparison, are rather fitted by three HN functions in addition to a power law term (Figure 7(b)). The third relaxation peak has less dielectric strength than the two other peaks, i.e. the MWS peak and the interfacial glass transition peak, and is most likely attributed to PS/PEB interphase region, which starts to be more important with increasing PS content.
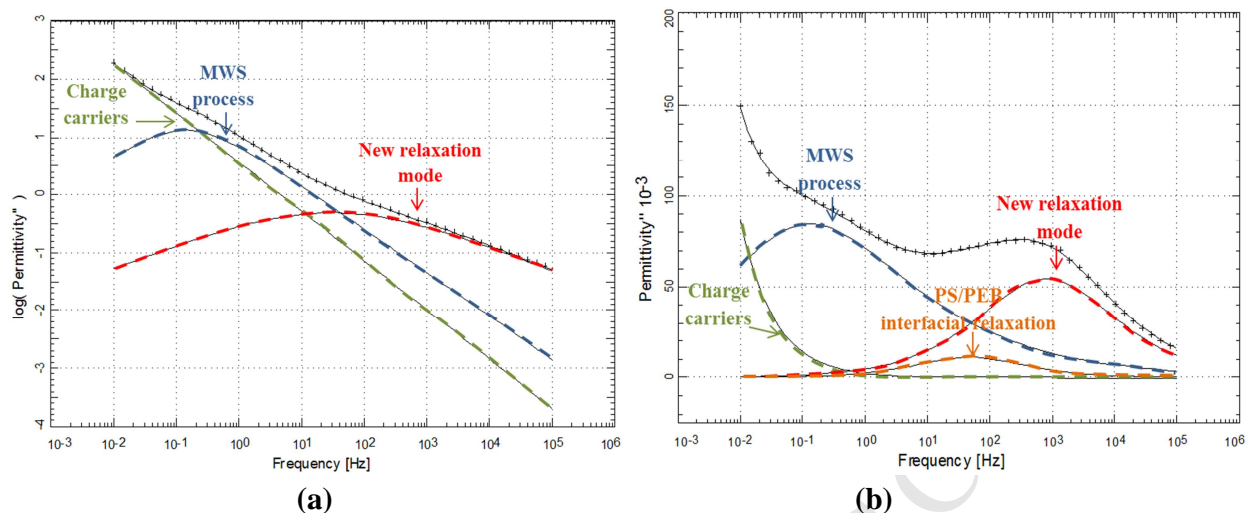
Figure 7. Examples of fitting according to equation (2) of respectively: (a) SEBS-13-20A-isotropic at

65 °C (ε" presented in log scale due to high contribution from charge fluctuation) and (b) SEBS-30-

20A-oriented at 70 °C (Different colors are used to denote the different contributions)

Relaxation times corresponding to the interfacial glass transition relaxation peak are plotted as a

function of temperature in Figure 8. The results corresponding to nanocomposites prepared from

SEBS-20 discussed earlier (Figure 6) are reported again for the sake of comparison. The VFT equations

corresponding to each sample are plotted as well, while the VFT parameters are summarized in Table 6.

In particular, SEBS-13 nanocomposites, featuring the lowest content of styrene, show similar values and

dependence on orientation of their interfacial T_{gi}, compared to samples prepared from SEBS-20, while

SEBS-30 nanocomposites, containing the highest fraction of styrene, show the lowest values and

sensitivity to orientation featuring T_{gi} values in the range of 6 to 9 °C. The fragility index values confirm

this observation as well. This fact might indicate that although clay nanoparticles exhibit more affinity to

the aromatic rings in PS blocks[1], they affect more the mobility of chains in the rubbery PEB phase, and

consequently are located more in contact with this phase. This latter observation is consistent with TEM

images reported in Figure 3(d)-(e), showing the presence of intercalated nanoclay that either cross PS

cylinders or are located completely outside PS cylinders if they are relatively big. Another possible reason could be related to the cylinder diameter, which is reduced with decreasing PS block content, providing more space for the contact between the clay nanoparticles and the PEB blocks. In fact, the diameter of PS cylinders in SEBS-13 is estimated to be equal to 9.7 nm according to calculations based on SAXS results (not reported in the manuscript), while in SEBS-20 and SEBS-30, the estimated diameter is respectively equal to 12.5 nm, according to the TEM image reported in Figure 3(e), and 13.5 nm according to a TEM image reported in reference[2]. As a consequence, in samples prepared from SEBS-30, the contact volume between clay nanoparticles and rubber chains might be reduced by the increased diameter of glassy PS rods, in a similar way in both oriented and isotropic samples, resulting in less sensitivity to orientation.

From another point of view, it could be seen that the relaxation times corresponding to SEBS-13 and SEBS-30 nanocomposites are both smaller than those corresponding to SEBS-20 nanocomposites. This behavior could be partially related to the bulk glass transition temperature of PEB phase, which might depend on its overall fraction in the block copolymer. In fact, the T_g of a specific block is usually different from the glass transition temperature of the corresponding homopolymer, and it depends on the interphase region between the blocks. In general, only when the compatibility between the blocks of a block copolymer is weak, a sharp interface is observed due to strong segregation and the T_g of each block is equal to the T_g of the corresponding homopolymer[69]. However, in the case of SEBS, the pendant groups of the hard PS phase might be mixed to the soft PEB phase forming an interphase region, as predicted from the small relaxation peak observed in SEBS-30 (Figure 7(b)). It will be shown later, by DMA measurements, that the Tg of each block increases with increasing fraction of that block in SEBS block copolymer.

In general, it is expected that the block copolymer matrices featuring higher bulk T_g of their PEB phase exhibit higher interfacial glass transition temperature and slower dynamics at a given temperature above the T_{gi}, if other factors such as the orientation and the interaction of nanoparticles with the block copolymer phases are maintained unchanged. This behavior is partially achieved. In fact, SEBS-30 based nanocomposites exhibit the lowest bulk T_g of the PEB block as what will be shown later by DMA, and simultaneously the fastest interfacial dynamics and the lowest T_{gi} compared to materials prepared from SEBS-13 and SEBS-20. However, one should keep in mind that the motion of polymer chains at the interphase region does not depend only on the corresponding bulk T_g of the rubber phase, but it depends also on other parameters including the interaction of nanoparticles with each block and the orientation as concluded earlier.
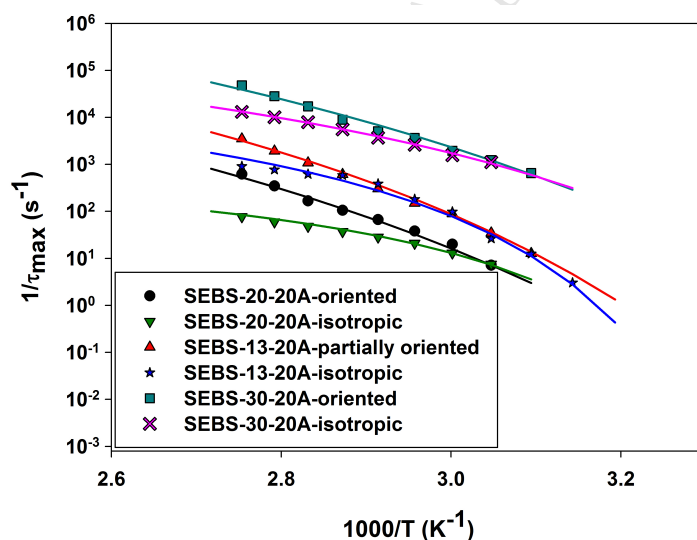
Figure 8. Temperature dependence of the relaxation times corresponding to SEBS-13 and SEBS-30 nanocomposites prepared by different processes: symbols correspond to relaxation times retrieved from the HN function and solid lines correspond to VFT fitting, plots corresponding to SEBS-20 nanocomposites are presented again for comparison

Table 6. VFT fitting parameters corresponding to SEBS-13 and SEBS-30 based nanocomposites

Samples	τ_0 (s)	T_0 (K)	B (K)	T_{gi} (K)	F
SEBS-13-20A- partially oriented	6.80E-09	244	1280	299	55.4
SEBS-13-20A-isotropic	7.16E-06	284	366	307	94.8
SEBS-30-20A-oriented	5.70E-10	220	1530	279	53.3
SEBS-30-20A-isotropic	2.59E-07	250	642	282	76.8

Effect of nanoparticles location and intercalation degree

To further understand the effect of the nanoparticles contact with one block or another on the observed interfacial peak, samples where nanoparticles are completely located in PEB phase are studied and compared to the previous results. The affinity of nanoparticles to PEB phase was increased by the attachment of maleic anhydride (MA) to it. MA exhibits great compatibility with the organic groups attached on the nanoparticles surface. Furthermore, this increased affinity results in more pronounced intercalation of the elastomer chains in clay galleries, disrupting the regular stacked layer structure of the organoclays and giving rise to mostly exfoliated structure, as reported in our previous study[2] (TEM micrographs of SEBS-30-MA-20A nanocomposites exhibiting exfoliated structure are available in Figure S6 of the ESI file, annex V). Hence, a higher fraction of elastomer chains is expected to be involved in this interphase region compared to the samples prepared without MA. The comparison of relaxation times between SEBS-30-20A and SEBS-30-MA-20A samples, plotted in Figure 9, shows that the presence of MA attached to the rubber phase affected remarkably the dynamics of the interphase region. In particular, relaxation times increased in the sample containing the MA graft, which indicates slower dynamics. This behavior is expected due to the selective location of clay in the rubber phase, which increases the amount of elastomer chains attached to the interface. In addition, the degree of clay exfoliation is improved in the presence of MA, which results in a larger number of interfaces and less efficient restriction of chains motion compared to intercalated structures. Hence, the cooperativity of interfacial chains is higher, resulting in increased relaxation times[60]. These hypotheses are in agreement

with the increased estimated T_{gi} equal to 20 °C for SEBS-30-MA-20A, when compared to 6 °C for the sample prepared without MA. These values were extrapolated from the VFT fitting parameters reported in Table 7. The comparison of the dielectric strength values of the two nanocomposites reported in Table 8 supports the same conclusion as well. In fact, the dielectric strength of the sample containing MA is considerably higher than that of the nanocomposite without MA.

Table 7. VFT fitting parameters corresponding to SEBS-30-MA-20A-oriented nanocomposite

Samples	τ_0 (s)	T_0 (K)	B (K)	T_{gi} (K)	F
SEBS-30-MA-20A-oriented	7.91E-10	237	1430	293	58.7

Table 8: Dielectric strength corresponding to SEBS-30-20A vs. SEBS-30-MA-20A nanocomposites prepared by extrusion

Samples	Δε at 60°C	Δε at 80°C
SEBS-30-20A-oriented	0.252	0.233
SEBS-30-MA-20A-oriented	0.865	0.830
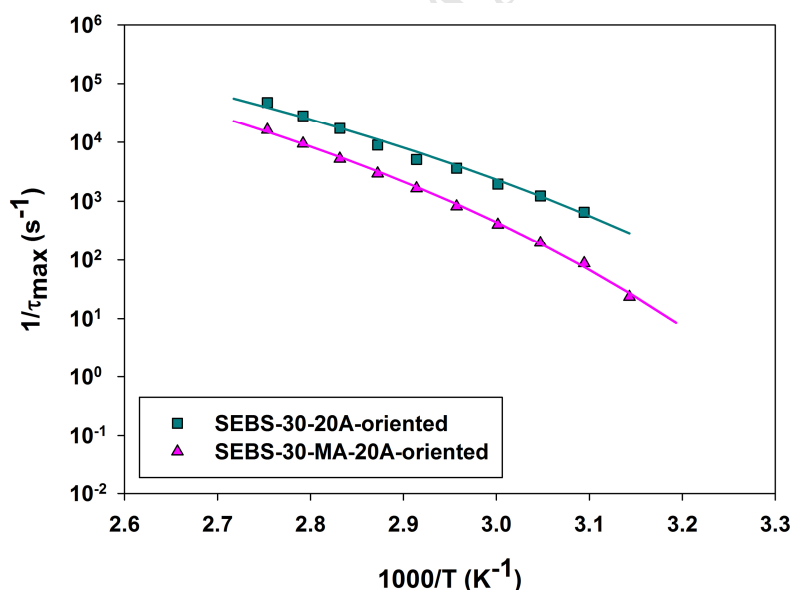
Figure 9. Temperature dependence of the relaxation times corresponding to SEBS-30-MA-20A-oriented nanocomposite: symbols correspond to relaxations times retrieved from the HN function and solid lines correspond to VFT fitting, plot corresponding to SEBS-30-20A-oriented nanocomposite are presented again for comparison

Overall, BDS data revealed the appearance of a new relaxation mode attributed to rubber chains with restricted mobility located at polymer/nanoparticle interfaces, in all the nanocomposites prepared from SEBS-13, SEBS-20, SEBS-30 and SEBS-MA-30 grades. A T_{gi} associated with this process is estimated to occur in the range 6 to 35 °C depending on the nanocomposite morphology. To confirm the molecular origin of this relaxation process, DMA was performed. Results will be discussed in the following section.

Dynamic mechanical analysis

Dielectric spectroscopy data discussed in this paper were mainly performed in the temperature range from 30 to 90 °C and analyzed as a function of frequency. In order to extend the study of relaxation phenomena to lower temperatures, to confirm the origin of the new relaxation peak observed in BDS and to evaluate the dependence of bulk glass transition temperatures of both PS and PEB blocks, respectively T_{gPEB} and T_{gPS}, on styrene fraction and clay addition, dynamic mechanical analysis was carried out in a large temperature range from -100 °C to 130 °C. In fact, in this range, both T_{gPEB} and T_{gPS} are expected to appear as peaks in DMA tan δ graphs. Besides, any potential peak that will appear in addition will be certainly due to a molecular relaxation, by contrast to BDS spectra, where relaxation phenomena observed in hybrid materials could be due to either a molecular origin or separation of charges at inner dielectric boundary layers (MWS polarization).

Figure 10 shows tan δ graphs corresponding to selected samples prepared from SEBS-30 (graphs corresponding to samples from SEBS-13 and SEBS-20 are not reported). It is worth noting that the DMA measurements were conducted in the transverse direction for all the studied samples (perpendicular to the main direction of PS cylinders alignment). In general, all curves show evidence of two peaks which correspond to T_{gPEB} (at low temperatures) and T_{gPS} (at high temperature). The values of T_{gPEB} and T_{gPS} corresponding to each material are reported in Table 9, except T_{gPS} corresponding to

SEBS-13 samples where no clear peaks were observed up to 130 °C. In a general trend, the glass transition temperature of each block, either PS or PEB, and the height of its corresponding peak increases with increasing fraction of that block in SEBS. This behavior is due to the fact that more chains of the considered block are involved in the glass transition phenomena leading to a larger damping. Besides, the T_g temperature and the intensity of the peak depend on the orientation of PS cylinders. Indeed, T_{gPS} of SEBS-20- partially oriented R1 material prepared by film blowing is 6 degrees higher than SEBS-20-oriented, 106 °C vs.100 °C. Simultaneously, the intensity of T_{gPS} is reduced and that of T_{gPEB} is considerably higher. This behavior might be due to the fact that these samples are not completely aligned in the extrusion direction which leads to an increasing fraction of PEB chains in the transverse direction, which is the direction of the test, as well as more hindrance of PS chains mobility.

In the nanocomposites, the addition of clay results, in some cases, in the reduction of T_g peak height and the broadening of the peak, such as the peaks corresponding to T_{gPS} in both SEBS-30-20A-oriented and SEBS-30-MA-20A-oriented nanocomposites, as shown in Figure 10. These behaviors respectively indicate lower number of chains participating in the bulk glass transition and wider distribution of chains mobility due to the restriction of motion imposed by clay nanoparticles. In addition, the glass transition temperatures of both blocks are either maintained or shifted to higher or lower temperatures. Shifts of bulk T_g to both higher and lower temperatures have been reported in the literature. The experimental results reported in the literature are in general not conclusive due to the complex nature of various polymers and nanocomposites that were investigated23[,70]. Different reasons were suggested to explain the phenomena depending on the cases. In particular, the increase was mainly attributed to restriction of chain mobility at the interface[23], while the decrease was attributed to different reasons such as a specific form of mechanical coupling between the filler, the bound layer and the bulk rubber[71,72], an increase of mobility[73] or an increase of free volume and decrease of molecular packing density[74].
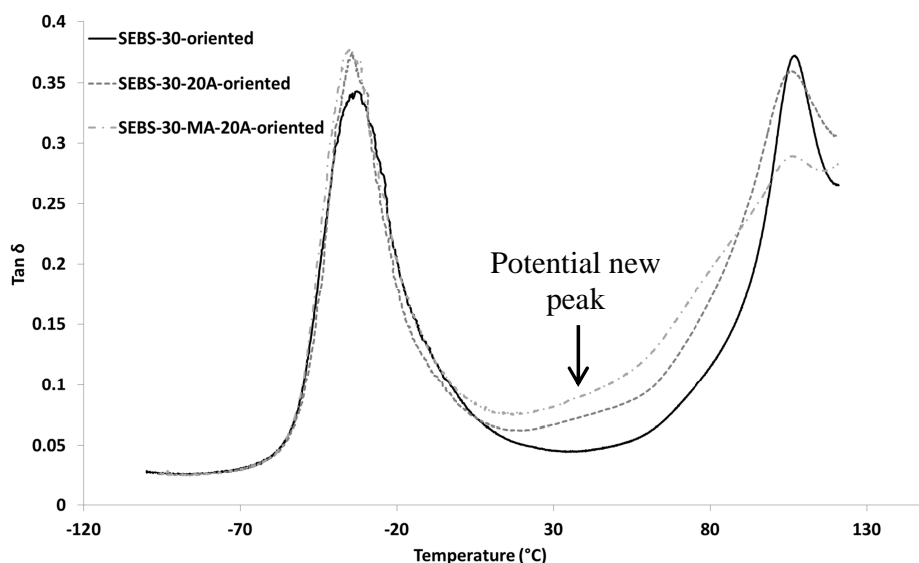
**Figure 10.** tan δ of different SEBS-30 materials (prepared by sheet die extrusion) from -100 °C to 130 °C at 1 Hz

Table 9: T_gs of both PS and PEB blocks in different samples of SEBS based nanocomposites

Sample	T_{gPEB} (°C)	T_{gPS} (°C)
SEBS-13-partially oriented	-23	-
SEBS-13-20A-partially oriented	-27	-
SEBS-20-oriented	-26	100
SEBS-20-20A-oriented	-26	100
SEBS-20- partially oriented R1	-26	106
SEBS-20-20A- partially oriented R1	-20	110
SEBS-30-oriented	-35	107
SEBS-30-20A-oriented	-34	105
SEBS-30-MA-20A- oriented	-33	104

In addition to the bulk glass transitions of PS and PEB blocks, nanocomposites prepared from SEBS-30 seem to exhibit an additional low intensity peak occurring at intermediate temperatures between T_{gPEB} and T_{gPS}, which might correspond to the glass transition of interfacial rubber chains with reduced mobility (as indicated by the arrow in Figure 10). However, this peak is not well resolved and as a consequence, resort to curve fitting was necessary. Although, there is no theoretical expression to describe dynamic mechanical relaxations as a function of temperature, the use of some empirical equations which reproduce satisfactorily the asymmetry of tan delta peaks has been reported in the

literature. One such is the exponentially modified Gaussian (EMG) which was used by **Tsagarapoulos et al.**[32] and **Cowie et al.**[75] to characterize T_g peaks and particularly peaks related to T_g of interfacial layers observed in several homopolymers containing relatively high fractions of fillers such as silica nanoparticles and cellulose tricarbanilate. Another model based on the three-parameter double sigmoid (ADS) equation was successfully used by **Arrighi et al.**[71] to characterize T_g of the interfacial layer observed in styrene butadiene rubber (SBR) containing silica nanoparticles.

In this study, we adopted a model based on ADS equation, similarly to reference[71], to describe both bulk T_g peaks and the new interfacial T_g peak. More details about this equation and its characteristic parameters are available in reference[71] and annex X of the ESI file (equation (S6)). The general model is composed of 3 ADS terms to describe the 3 peaks. An additional ADS term with a large asymmetry in the high temperature side was also considered to take into account the increasing baseline towards high temperatures. For consistency, the same parameters were taken for the baseline term in the neat SEBS-30-oriented and the nanocomposites. Examples of the fitting of both neat SEBS-30-oriented and SEBS-30-20A-oriented nanocomposites showing the resolved T_g peaks are reported in Figure 11.
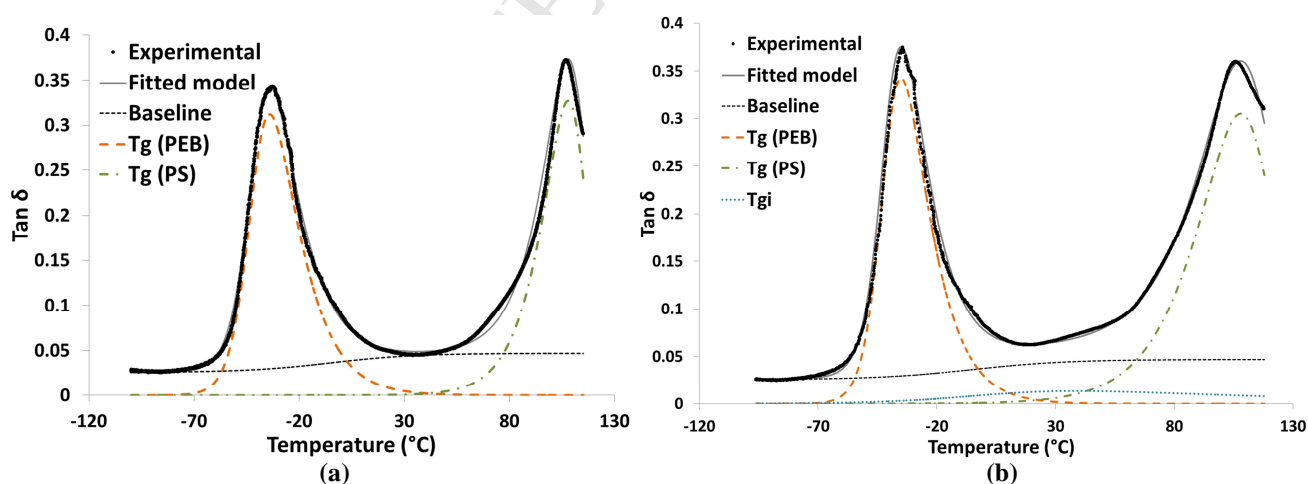
Figure 11. Fitted tan delta curves showing bulk T_gs of PS and PEB blocks as well as T_{gi} of the interfacial layer (an additional ADS term is considered for the increasing baseline): (a) SEBS-30-oriented and (b) SEBS-30-20A-oriented

The peak corresponding to the glass transition of the interfacial layer, T_{gi}, in both nanocomposites, resulting from the curve-fitting process, is characterized by low intensity and a broad shape indicating a large distribution of chains mobility in the interfacial layer. Temperatures corresponding to T_{gi} peaks maxima are reported in Table 10. Taking the difference between these values and T_{gPEB} values reported in Table 9, T_{gi} of the interfacial rubbery layer is estimated to occur 72 degrees higher than the bulk in the case of SEBS-30-20A-oriented and 86 degrees higher than the bulk in the case of SEBS-30-MA-20A-oriented. This result is consistent with many findings in the literature expecting the glass transition of tethered chains confined at the interface to occur 70 to 110 degrees higher than the bulk Tg^{32}. It is worth noting that these values of T_{gi} determined from DMA data at 1 Hz are higher than those estimated earlier by BDS through the extrapolation of the VFT equation at very low relaxation times (100s): 38 °C vs. 6 °C for SEBS-30-20A-oriented and 53 °C vs. 20 °C for SEBS-MA-30-20A-oriented. However, the trend is maintained. Hence, to check the similarity of the results given by both BDS and DMA techniques, dielectric permittivity of SEBS-30-oriented and SEBS-30-20A-oriented materials were mapped in an extended temperature range [-100, 150 °C] and dielectric loss spectra were plotted as function of temperature at 1 Hz (data available in the ESI file, annex IX). At this frequency, the peak corresponding to T_{gPEB} is observed at -45 °C, which is 10 degrees higher than DMA and the peak corresponding to T_{gi} is observed at 40 °C, which is 2 degrees higher than the value obtained by DMA. This difference between the results given by the two methods is observed even when equivalent formalisms are used: electric modulus vs. mechanical modulus. Thus, it is rather due to experimental conditions such as different heating rates[76].

The fraction of bound polymer chains participating in the interfacial glass transition, F_{Bound}, could be determined by dividing the area under T_{gi} peak by the sum of the areas of all T_g peaks. Values of integrated area under each peak and estimated bound fractions are reported Table 10 as well. The bound

fraction in SEBS-30-20A-oriented is around 7.5% while in SEBS-30-MA-20A-oriented, it is around 12%. This is expected as the higher degree of exfoliation in the latter nanocomposite results in more interfacial area. Taking into account data about the average particle size of clay nanoparticles in SEBS-30 nanocomposites, which were published previously by coauthors[1], the thickness of interfacial layer around each particle could be estimated in a similar fashion to the work of **Arrighi et al.**[71]. More details regarding this procedure could be consulted in annex X of the ESI file (equations (S7) to (S10)).

Table 10: Interfacial T_{gi}, bound fraction and interfacial layer thickness in SEBS-30 based

nanocomposites

| Sample	$T_{gi}(°C)$	A_{PEB}	A_{PS}	A_{Int}	F_{Bound}	T(nm)
SEBS-30-20A-oriented	38	9.475	10.15	1.59	0.075	10.5
SEBS-30-MA-20A-oriented	53	9.42	10.04	2.58	0.12	7.6

The average tactoid thickness, average lateral dimensions and average number of clay layers per tactoid were determined based on the TEM quantitative analysis of clay dimensions in SEBS-30-20A and SEBS-30-MA-20A nanocomposites reported by **Carastan et al.**[1]. These values are listed in Table 11.

Table 11: Average dimensions of clay tactoids based on TEM quantitative analysis published by **Carastan et al.**[1]

	Average thickness (nm)	Average lateral size (nm)	Average number of layers
SEBS-30-20A-oriented	7.3	243.3	3
SEBS-30-MA-20A-oriented	3	116.3	2

To calculate the thickness of the interfacial layer in both nanocomposites, the clay tactoid was considered as a solid particle surrounded on both lateral sides with constrained rubber chains. Since the thickness of one tactoid is much smaller than its lateral dimension, the fraction of chains that could be constrained along the thickness was neglected. Then, the calculated interfacial layer thickness, t, was adjusted to take into account that some chains are rather confined in the interlayer spacing, considering that the thickness of 1 clay layer is equal to 0.94nm[1].These approximations are illustrated in Figure 12.

With these approximations the calculated values of interfacial layer thickness are respectively equal to

7.6 nm for SEBS-30-MA-20A nanocomposite and 10.5 nm for SEBS-30-20A. They are in agreement

with findings from the literature which reported estimations of thickness of the interfacial layer.

Whether evaluated experimentally[23,71] or theoretically[27,28,77], the values reported in the literature did not

exceed few nanometers ranging from 2 to 10 nm in most of the reported studies.
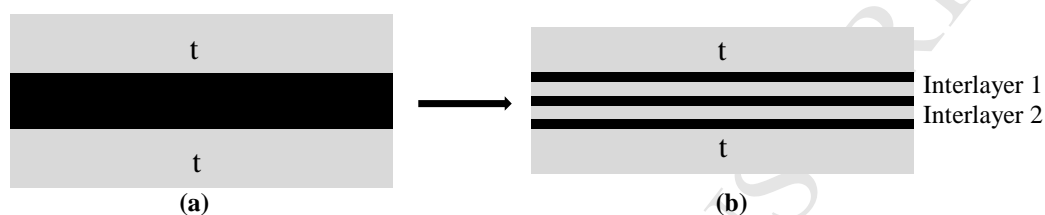
Figure 12. Scheme of the interfacial layer covering the lateral side of clay particles: (a) First

approximation: clay tactoid as a solid particle, (b) part of the interfacial layer is between clay galleries

Hence, the fitting model based on ADS equation describes satisfactorily the bulk glass transitions of

both PEB and PS blocks as well as the T_{gi} of interfacial chains with restricted mobility. It leads to an

approximation of the interfacial layer thickness well in agreement with values reported in the literature.

However, it is worth noting that an important hypothesis was assumed in the calculation of the

interfacial layer thickness, which is the absence of an immobilized layer corresponding to polymer

chains that are tightly bounded and don't participate in neither bulk T_g nor interfacial T_{gi}[32]. In fact, the

total number of chains participating in glass transition phenomena in a nanocomposite is generally lower

than the number of chains participating in the glass transition of the neat material. Thus, by comparing

the total area under Tg peaks in respectively the nanocomposite and the pure material, the fraction of

immobilized layer could be determined and excluded when calculating the thickness of the interfacial

layer[71]. The thickness of the immobilized layer was estimated in the literature to be in the range 0.5 to 2

nm[71]. In our case, comparing the tan delta curves of the neat SEBS-30 and its corresponding

nanocomposites, we could see that the total area is higher in the case of nanocomposites, which gives

the impression that more chains are involved in the glass transition phenomena compared to the neat copolymer. This behavior is puzzling and for this reason comparison with neat and estimation of the immobilized fraction were not possible. As a consequence, the estimated thicknesses of the interfacial layer might be smaller in reality. Another behavior that requires more investigation is the fact that the T_{gi} peak related to interfacial rubbery chains was not observed in SEBS-13 and SEBS-20 nanocomposites by DMA, by contrast to BDS. Only shifts of bulk T_g temperatures were obvious by this technique. However, for nanocomposites prepared from SEBS-30 and SEBS-30-MA, the new relaxation process was confirmed by both DMA and BDS. Furthermore, T_{gi} temperatures estimated by both techniques were in agreement.

V) Concluding remarks

In this study, nanocomposites of SEBS block copolymer with cylindrical morphology and organically modified clay nanoparticles have been successfully prepared with different configurations of PS cylinders and clay nanoparticles. In particular, isotropic vs. oriented vs. partially oriented morphologies have been successfully prepared by different processing techniques and confirmed by SAXS and TEM.

In all the nanocomposites, a glassy interphase region was formed and gave rise to a new relaxation mode corresponding to the interfacial rubbery chains with restricted mobility.

A dielectric "interfacial" glass transition T_{gi}, associated with this process, is estimated to occur at temperatures ranging from 6 up to 35 °C, depending on the orientation of both PS domains and clay nanoparticles, the fraction of polystyrene block as well as the location and the degree of exfoliation of clay nanoparticles, which was tuned through the use of maleic anhydride graft. The thickness of the interfacial layer was estimated through fitting of DMA data and was found to be in the range 7.5-10.6 nm for nanocomposites prepared from SEBS-30 and SEBS-30-MA.

Overall, the relaxation mode related to this interphase region was sensitive to the following key parameters:

- Distribution of interfaces: oriented vs. isotropic vs. partially oriented; which affects the area and the volume of the "interphase region" as well as the mobility of polymer chains. In particular, samples featuring random or partially oriented morphologies were found to exhibit higher interaction, dielectric strength and T_{gi}, up to 9 degrees higher, compared to their oriented counterparts. Besides, partially oriented samples prepared by film blowing extrusion featured the most "fragile" behavior and the fastest dynamics at temperatures above estimated T_{gi}, compared to oriented and isotropic samples. This behavior could be attributed to suppression of cooperativity of interfacial chains motion due to strong confinement in this configuration.

- Ratio of PS/PEB, which affects the T_g of the bulk PEB block, the diameter of PS cylinders as well as the amount and the mobility of PEB chains located in the interphase region. In particular, the T_{gi} was found to decrease and to be less sensitive to orientation effects, with increasing styrene content, most likely due to reduced amount of rubber chains involved in the interphase region and increasing diameter of PS cylinders resulting in a similar trend of confinement in both oriented and non-oriented samples.

- Location of clay nanoparticles either in PS or PEB blocks, which was modulated by the use of maleic anhydride attached to the rubber phase. In particular, in the presence of MA, clay particles were located exclusively within the elastomer block, resulting in increased amount of rubber chains involved in the interphase region and consequently higher dielectric strength associated to the relaxation process. Moreover, the degree of exfoliation of clay tactoids is improved, which induced slower dynamics compared to intercalated structures where strongly confined rubber chains exhibit reduced cooperativity and consequently reduced relaxation times.

Finally, the charge fluctuation contribution to the dielectric loss was dependent as well on the morphology. In particular, the conduction loss was reduced by 2 to 4 orders of magnitude in the samples with controlled architecture, i.e. oriented and partially oriented, as clay nanoparticles were quasi-aligned perpendicular to the electric field in these configurations.

Associated content

Supporting electronic information (ESI) file: 2D and 1D SAXS patterns, TEM micrographs and dielectric spectroscopy data related to the studied nanocomposites are available. The procedure of the estimation of the interfacial layer thickness is explained as well.

Author information

Corresponding Author: Nicole R. Demarquette, Department of Mechanical Engineering, École de Technologie Supérieure, 1100 rue Notre Dame, H3C 1K3 Montreal, Canada.

E-mail: NicoleR.Demarquette@etsmtl.ca, Phone: (001) 514 396-8658

References

(1) D.J. Carastan, L.G. Amurin, A.F. Craievich, M.C. Gonçalves, N.R. Demarquette, Clay-containing block copolymer nanocomposites with aligned morphology prepared by extrusion, Polym. Int., 2014, Vol. 63 (2), pp. 184–194.

(2) E. Helal, N.R. Demarquette, L.G. Amurin, E. David, D.J. Carastan and M. Fréchette, Styrenic block copolymer-based nanocomposites: Implications of nanostructuration and nanofiller tailored dispersion on the dielectric properties, Polymer, 2015, Vol. 64, pp. 139–152.

(3) P.S. Goh, A.F. Ismail and B.C. Ng, Directional alignment of carbon nanotubes in polymer matrices: Contemporary approaches and future advances, Composites, Part A, 2014, Vol. 56, pp. 103–126.

(4) T. Terao et al., Alignment of boron nitride nanotubes in polymeric composite films for thermal conductivity improvement, J. Phys. Chem. C, 2010. Vol. 114, pp. 4340-4344.

(5) Z. Cui, Z. Cao, R. Ma, A.V. Dobrynin, and D.H. Adamson, Boron Nitride Surface Activity as Route to Composite Dielectric Films, ACS Appl. Mater. Interfaces, 2015, Vol. 7 (31), pp 16913–16916.

(6) G. Galgali, S. Agarwal and A. Lele, Effect of clay orientation on the tensile modulus of polypropylene–nanoclay composites, Polymer, 2004, Vol. 45, pp. 6059–6069.

(7) E. David, M. Fréchette, B. Zazoum, C. Daran-Daneau, A. D. Ngô and H. Couderc, Dielectric Properties of PE/Clay Nanocomposites, J. Nanomater., Vol. 2013, Article ID 703940.

(8) V. Tomer, G. Polizos, C. A. Randall and E. Manias, Polyethylene nanocomposite dielectrics: Implications of nanofiller orientation on high field properties and energy storage, J. Appl. Phys., 2011, Vol. 109, 074113.

(9) S.P. Fillery, H. Koerner, L. Drummy, E. Dunkerley, M.F. Durstock, D.F. Schmidt and R.A. Vaia, Nanolaminates: Increasing Dielectric Breakdown Strength of Composites, ACS Appl. Mater. Interfaces, 2012, 4 (3), pp 1388–1396.

(10) R.A. Vaia and J.F. Maguire, Polymer Nanocomposites with Prescribed Morphology: Going beyond Nanoparticle-Filled Polymers, Chem. Mater., 2007, Vol. 19, Issue 11, pp. 2736–2751.

(11) E. Helfand, Block Copolymer Theory. III. Statistical Mechanics of the Microdomain Structure, Macromolecules, 1975, Vol. 8, pp. 552–556.

(12) T. Ohta and K. Kawasaki, Comment on the free energy functional of block copolymer melts in the strong segregation limit, Macromolecules, 1990, Vol. 23, pp 2413–2414.

(13) A. N. Semenov, Theory of block copolymer interfaces in the strong segregation limit, Macromolecules, 1993, Vol. 26, pp. 6617–6621.

(14) I.W. Hamley, Structure and flow behaviour of block copolymers, J. Phys.: Condens. Matter, 2001, Vol.13, R643-R671.

(15) B. Sarkar and P. Alexandridis, Block copolymer–nanoparticle composites: Structure, functional properties, and processing, Prog. Polym. Sci., 2015, Vol. 40, pp. 33–62.

(16) M. Fréchette et al., Functional Nanomaterials For Electric Power, WG D1.40 (Beta version), International Council for Large Electric Systems (CIGRE) publication, May 2015.

(17) F. Kremer and A. Schönhals, Broadband dielectric spectroscopy, Book Chapters 3, 7 and 13, Springer Edition, 2003.

(18) M. Roy, J.K. Nelson, R.K. MacCrone, L.S. Schadler, C.W. Reed, R. Keefe and W. Zenger, Polymer Nanocomposite Dielectrics – The Role of the Interface, IEEE Trans. Dielectr. Electr. Insul., 2005, Vol. 12, pp. 629-643.

(19) L.A. Utracki, Clay-Containing Polymeric Nanocomposites and Their Properties, IEEE Electrical Insulation Magazine, 2010, Vol. 26, pp. 6-15.

(20) L.T. Vo, S.H. Anastasiadis and E.P. Giannelis, Dielectric study of Poly(styrene-co-butadiene) Composites with Carbon Black, Silica and Nanoclay, Macromolecules, 2011, Vol. 44 (15), pp. 6162–6171.

(21) M. Hernández, J. Carretero-González, R. Verdejo, T. A. Ezquerra and M. A. López-Manchado, Molecular dynamics of Natural Rubber/Layered Silicate Nanocomposites As Studied by Dielectric Relaxation Spectroscopy, Macromolecules, 2010, Vol. 43, pp. 643–651.

(22) M. Qu, F. Deng, S. M. Kalkhoran, A. Gouldstone, A. Robisson and K.J. Van Vliet, Nanoscale visualization and multiscale mechanical implications of bound rubber interphases in rubber–carbon black nanocomposites, Soft Matter, 2011, Vol. 7, pp. 1066–1077.

(23) Y. Lin, L. Liu, G. Xu, D. Zhang, A. Guan, and G. Wu, Interfacial Interactions and Segmental Dynamics of Poly(vinylacetate)/Silica Nanocomposites, J. Phys. Chem. C, 2015, Vol. 119, pp. 12956–12966.

(24) P. Klonos, A. Kyritsis and P. Pissis, Interfacial dynamics of polydimethylsiloxane adsorbed on fumed metal oxide particles of a wide range of specific surface area, Polymer, 2015, Vol. 77, pp. 10-13.

(25) L. Chen, K. Zheng, X. Tian, K. Hu, R. Wang, C. Liu, Y. Li and P. Cui, Double Glass Transitions and Interfacial Immobilized Layer in in-Situ-Synthesized Poly(vinyl alcohol)/Silica Nanocomposites, Macromolecules, 2010, Vol. 43 (2), pp. 1076–1082.

(26) C.G. Robertson and M. Rackaitis, Further Consideration of Viscoelastic Two Glass Transition Behavior of Nanoparticle-Filled Polymers, Macromolecules, 2011, Vol. 44 (5), pp. 1177–1181.

(27) Y. Gao, J. Liu, L. Zhang and D. Cao, Existence of a Glassy Layer in the Polymer-Nanosheet Interface: Evidence from Molecular Dynamics, Macromol. Theory Simul. 2014, Vol. 23, pp. 36–48.

(28) A. Ghanbari, M. Rahimi and J. Dehghany, Influence of Surface Grafted Polymers on the Polymer Dynamics in a Silica-Polystyrene Nanocomposite: A Coarse-Grained Molecular Dynamics Investigation, J. Phys. Chem. C, 2013, Vol. 117, pp. 25069-25076.

(29) A.P. Holt, P.J. Griffin, V. Bocharova, A.L. Agapov, A.E. Imel, M.D. Dadmun, J.R. Sangoro and A.P. Sokolov, Dynamics at the Polymer/Nanoparticle Interface in Poly(2-vinylpyridine)/Silica Nanocomposites, Macromolecules, 2014, Vol. 47 (5), pp.1837–1843.

(30) M. Hernández, M. del Mar Bernal, R. Verdejo, T.A. Ezquerra and M.A. López-Manchado, Overall performance of natural rubber graphene nanocomposites, Compos. Sci. Technol., 2012, Vol. 73, 23, pp. 40–46.

(31) G. Tsagaropoulos and A. Eisenburg, Direct observation of two glass transitions in silica-filled polymers: Implications to the morphology of random ionomers, Macromolecules, 1995, Vol. 28, pp. 396–398.

(32) G. Tsagaropoulos and A. Eisenburg, Dynamic Mechanical Study of the Factors Affecting the Two Glass Transition Behavior of Filled Polymers: Similarities and Differences with Random Ionomers, Macromolecules, 1995, Vol. 28, pp 6067–6077.

(33) F.W. Starr, T.B. Schrøder and S.C. Glotzer, Molecular Dynamics Simulation of a Polymer Melt with a Nanoscopic Particle, Macromolecules, 2002, Vol. 35, 4481- 4492.

(34) H. Chen, M.K. Hassan, S.K. Peddini and K.A. Mauritz, Macromolecular dynamics of sulfonated poly(styrene-b-ethylene-ran-butylene-b-styrene) block copolymers by broadband dielectric spectroscopy, Eur. Polym. J., 2011, Vol. 47, pp. 1936–1948.

(35) G. Holden et al., Thermoplastic Elastomers, Book Chapter 3, Hanser Gardner Publications, 3rd Edition, 2004.

(36) V. Balsamo, A. T. Lorenzo, A. J. Müller, S. Corona-Galván, , L. M. Fraga Trillo, and V. R. Santa Quiteria, Structure, Properties and Applications of ABA and ABC Triblock Copolymers with Hydrogenated Polybutadiene Blocks, Block Copolymers in Nanoscience, Book Chapter 16, pp. 367-389, John Wiley and Sons, 2008.

(37) J. Liu, V. Mhetar and J. Freestone, Insulation containing styrene copolymers, United States Application Publication, US0308836 A1, 2011.

(38) Z. Ma et al., Effect of styrene–ethylene–butadiene–styrene and its synergetic effect with ethylene vinyl acetate on the mechanical, thermal, dielectric, and water-treeing behaviors of crosslinked polyethylene, J. Appl. Polym. Sci., 2010, Vol. 118, pp. 2350-2357.

(39) B. Kim, Y.D. Park, K. Min, J.H. Lee, S.S. Hwang, S.M. Hong, B.H. Kim, S.O. Kim and C.M. Koo, Electric Actuation of Nanostructured Thermoplastic Elastomer Gels with Ultralarge Electrostriction Coefficients, Adv. Funct. Mater., 2011, Vol. 21, Issue 17, pp. 3242–3249.

(40) M. F. Fréchette et al., Nanostructured polymer microcomposites: A distinct class of insulating materials, IEEE Trans. Dielectr. Electr. Insul., 2008, Vol. 15, pp. 90-105.

(41) M.F. Fréchette, M.L. Trudeau, H.D. Alamdari and S. Boily, Introductory Remarks on Nanodielectrics, IEEE Trans. Dielectr. Electr. Insul., 2004, Vol. 11, No. 5, pp. 808-818.

(42) R.R. De Sousa Jr., L.G. Amurin, N. R. Demarquette and D.J. Carastan, Block copolymer nanocomposites with mono- and bioriented structures, Technical Proceedings of the 2014 NSTI Nanotechnology Conference and Expo NSTI-Nanotech, 2014, Vol. 1, pp. 412-415.

(43) L.G. Amurin, D.J. Carastan and N.R. Demarquette, Morphological evolution of block copolymer nanocomposites submitted to extrensional flows, J. Rheol., 2016, Vol. 60, pp. 175-189.

(44) N. Hadjichristidis, A. Hirao, Y. Tezuka and F. Du Prez, Complex macromolecular architectures: synthesis, characterization and self-assembly, Book Chapter 25, John Wiley & Sons, 2011.

(45) D.J. Carastan, N.R. Demarquette, A. Vermogen and K. Masenelli-Varlot, Linear viscoelasticity of styrenic block copolymers–clay nanocomposites, Rheol. Acta, 2008, Vol. 47, Issue 5, pp 521-536.

(46) D.J. Carastan, , L.G. Amurin, , A.F. Craievich, , M.C. Gonçalves, , N.R. Demarquette, , Morphological evolution of oriented clay-containing block copolymer nanocomposites under elongational flow,   Eur. Polym. J., 2013, Vol. 49, Issue 6, pp.1391–1405.

(47) A. K. Jonscher, Universal relaxation law: a sequel to Dielectric relaxation in solids, Chelsea Dielectrics Press, 1996.

(48) A. K. Jonscher, Dielectric relaxation in solids, Chelsea Dielectrics Press, 1983.

(49) S. Havriliak and S. Negami, A Complex Plane Representation of Dielectric and Mechanical Relaxation Processes in Some Polymers, Polymer, 1967, Vol. 8, pp. 161-210.

(50) G. Kofod, S. Risse, H. Stoyanov, D.N. McCarthy, S. Sokolov and R. Kraehnert, Broad-Spectrum Enhancement of Polymer Composite Dieletric Constant at Ultralow Volume Fractions of Silica-Supported Copper Nanoparticles, ACS Nano, 2011, Vol. 5, pp. 1623–1629.

(51) T. Blythe and D. Bloor, Electrical Properties of Polymers, Cambridge University Press, Second Edition, 2008.

(52) J. Tokarský, L. Kulhánková, L. Neuwirthová, K.M. Kutláková, S. Vallová, V. Stýskala and P. Čapková, Highly anisotropic conductivity of tablets pressed from polyaniline-montmorillonite nanocomposite, Mater. Res. Bull., 2016, Vol. 75, pp. 139–143.

(53) F. Uddin, Clays, Nanoclays, and Montmorillonite Minerals, Metall. Mater. Trans. A, 2008, Vol. 39, pp. 2804-2814.

(54) E. David and M. Fréchette, Polymer Nanocomposites - Major Conclusions and Achievements reached so far, IEEE Electrical Insulation Magazine, 2013, Vol. 20, pp. 29-36.

(55) H. Saleem, , M. Thunga, M. Kollosche, M.R. Kessler, S. Laflamme, Interfacial treatment effects on behavior of soft nano-composites for highly stretchable dielectrics, Polymer, 2014, Vol. 55, Issue 17, pp. 4531–4537.

(56) T. Glaskova and A. Aniskevich, Moisture absorption by epoxy/montmorillonite nanocomposite, Compos. Sci. Technol., 2009, Vol. 69, pp. 2711–2715.

(57) I. Preda , H. Couderc, M. Fréchette, S. Savoie, F. Gao, R. Nigmatullin, S.Thompson, J. Castellon, Dielectric response of modified epoxy/clay nanocomposites, IEEE Conf. Electr. Insul. Dielectr. Phenom. (CEIDP), 2012, pp. 531-534.

(58) R.N. Darie, E. Pâslaru, A. Sdrobis, G.M. Pricope, G.E. Hitruc, A. Poiată, A. Baklavaridis and C. Vasile, Effect of Nanoclay Hydrophilicity on the Poly(lactic acid)/Clay Nanocomposites Properties, Ind. Eng. Chem. Res., 2014, Vol. 53 (19), pp 7877–7890.

(59) E. David, B. Zazoum, M.F. Fréchette and F. Rogti, Dielectric Response of HDPE/Clay Nanocomposites Containing 10%wt of Organo-Modified Clay, IEEE Conf. Electr. Insul. Dielectr. Phenom. (CEIDP), 2015, pp.531-534.

(60) S. Wu, Z. Tang, Baochun Guo, Liqun Zhang and Demin Jia, Effects of interfacial interaction on chain dynamics of rubber/graphene oxide hybrids: a dielectric relaxation spectroscopy study, RSC Advances, 2013, Vol. 3, pp. 14549–14559.

(61) C.A Angell, Relaxation in liquids, polymers and plastic crystals — strong/fragile patterns and problems, J. Non-Cryst. Solids, 1991, Vol.131–133, pp. 13-31.

(62) R. Böhmer, K. L. Ngai, C. A. Angell and D. J. Plazek, Non exponential relaxations in strong and fragile glass formers, J. Chem. Phys., 1993, Vol. 99, pp. 4201.

(63) A. Schönhals, H. Goering, C. Schick, B. Frick and R. Zorn, Glass transition of polymers confined to nanoporous glasses, Colloid Polym. Sci., 2004, Vol. 282, pp. 882-891.

(64) I. Preda, J. Castellon, S. Agnel, H. Couderc, M. Fréchette, F. Gao, R. Nigmatullin, S.Thompson, A.-F. Vaessen, Dielectric Response of Various Partially Cured Epoxy Nanocomposites, IEEE Trans. Dielectr. Electr. Insul., 2013, Vol. 20, pp. 580-591.

(65) R. Böhmer and C.A. Angell, Disorder Effects on relaxational Processes, Springer, Berlin, Germany, 1994.

(66) T.A. Vilgis, Strong and fragile glasses: A powerful classification and its consequences, Phys. Rev. B, 1993, Vol. 47, pp. 2882-2885.

(67) J.G. Kirkwood, The Dielectric Polarization of Polar Liquids, J.Chem. Phys, 1939, Vol. 7, pp. 911–919.

(68) H. Frohlich, Theory of Dielectrics: Dielectric Constant and Dielectric Loss; Clarendon Press: Oxford, 1949.

(69) R. Adhikari, Correlations between Molecular Architecture, Morphology and Deformation Behaviour of Styrene/Butadiene Block Copolymers and Blends, Chapter 4, PhD Thesis presented to Martin-Luther-University Halle-Wittenberg, 2001.

(70) P. Rittigstein, J.M. Torkelson, Polymer–nanoparticle interfacial interactions in polymer nanocomposites: Confinement effects on glass transition temperature and suppression of physical aging, J. Polym. Sci., Part B: Polym. Phys.2006,44, 2935–2943.

(71) V. Arrighi, I.J. McEwen, H. Qian and M.B. Serrano Prieto, The glass transition and interfacial layer in styrene-butadiene rubber containing silica nanofiller, Polymer, 2003, 44, pp. 6259-6266.

(72) P. Mélé, S. Marceau, D. Brown, Y. de Puydt, N. D. Albérola, Reinforcement effects in fractal-structure-filled rubber, Polymer, Volume 43, Issue 20, 1 September 2002, pp. 5577–5586.

(73) N. Hao, M. Böhning and A. Schönhals, Dielectric Properties of Nanocomposites Based on Polystyrene and Polyhedral Oligomeric Phenethyl-Silsesquioxanes, Macromolecules 2007,40, 9672-9679.

(74) N. Hao , M. Böhning , H. Goering and A. Schönhals, Nanocomposites of Polyhedral Oligomeric Phenethylsilsesquioxanes and Poly(bisphenol A carbonate) as Investigated by Dielectric Spectroscopy, Macromolecules, 2007, 40 (8), pp 2955–2964.

(75) J.M.G. Cowie, V. Arrighi, J. Cameron and D. Robson, Lyotropic liquid crystalline cellulose derivatives in blends and molecular composites, Macromolecular Symposia 2000, Vol. 152, pp.107-116.

(76) R.A . Talja and Y.H. Roos, Phase and state transition effects on dielectric, mechanical and thermal properties of polyols, Thermochimica Acta, Vol. 380 (2), pp. 109–121, 2001.

(77) T. Heid, Innovative nanostructured epoxy composites for enhanced high voltage systems, PhD Thesis presented to École de Technologie Supérieure, 2015.

- Morphology of clay/thermoplastic elastomer can be tailored by processing
- Isotropic, totally oriented and partially oriented nanocomposites were obtained
- Identification of additional relaxation of rubber chains at clay/polymer interfaces
- New relaxation depends on the orientation of clay and copolymer nanodomains
- New relaxation corresponds to an interfacial layer of thickness around 7 to 10 nm